

Schwinger boson theory of ordered magnets

Shang-Shun Zhang ^{1,2}, E. A. Ghioldi,¹ L. O. Manuel ³, A. E. Trumper ³ and Cristian D. Batista ^{1,4}¹*Department of Physics and Astronomy, The University of Tennessee, Knoxville, Tennessee 37996, USA*²*School of Physics and Astronomy and William I. Fine Theoretical Physics Institute, University of Minnesota, Minneapolis, Minnesota 55455, USA*³*Instituto de Física Rosario (CONICET) and Universidad Nacional de Rosario, Boulevard 27 de Febrero 210 bis, (2000) Rosario, Argentina*⁴*Quantum Condensed Matter Division and Shull-Wollan Center, Oak Ridge National Laboratory, Oak Ridge, Tennessee 37831, USA*

(Received 9 September 2021; revised 8 May 2022; accepted 25 May 2022; published 13 June 2022)

The Schwinger boson theory provides a natural path for treating quantum spin systems with large quantum fluctuations. In contrast to semiclassical treatments, this theory allows us to describe a continuous transition between magnetically ordered and spin liquid states, as well as the continuous evolution of the corresponding excitation spectrum. The square lattice Heisenberg antiferromagnet is one of the first models that was approached with the Schwinger boson theory. Here we revisit this problem to reveal several subtle points that were omitted in previous treatments and that are crucial to further develop this formalism. These points include the freedom for the choice of the saddle point (Hubbard-Stratonovich decoupling and choice of the condensate) and the $1/N$ expansion in the presence of a condensate. A key observation is that the spinon condensate leads to Feynman diagrams that include contributions of different order in $1/N$, which must be accounted for to get a qualitatively correct excitation spectrum. We demonstrate that a proper treatment of these contributions leads to an exact cancellation of the single-spinon poles of the dynamical spin structure factor, as expected for a magnetically ordered state. The only surviving poles are the ones arising from the magnons (two-spinon bound states), which are the true collective modes of an ordered magnet.

DOI: [10.1103/PhysRevB.105.224404](https://doi.org/10.1103/PhysRevB.105.224404)

I. INTRODUCTION

Spin wave theory (SWT) is the traditional approach to describe the low-temperature properties of magnetically ordered states. This semiclassical approach, which is based on a $1/S$ expansion and becomes exact in the $S \rightarrow \infty$ limit, is indeed adequate to describe the low-energy excitation spectrum of Heisenberg models, whose magnetically ordered ground states have small quantum fluctuations. As is well known, quantum fluctuations can be enhanced by different factors, such as low-spin, low-dimensionality, and frustration, which guide the search for quantum spin liquids in real materials. This ongoing search is revealing multiple examples of magnets whose excitation spectrum is not captured by a $1/S$ expansion despite the fact that their ground state is magnetically ordered. It is then necessary to develop alternative approaches that can capture the strong quantum effects revealed by the excitation spectrum of these materials.

The Schwinger boson theory (SBT) introduced by Arovas and Auerbach [1,2] provides an alternative path for modeling magnets with strong quantum fluctuations. The Schwinger boson (SB) representation of spin operators allows one to reformulate the Heisenberg model as a quartic Hamiltonian of spin-1/2 bosons subject to the local constraint of $2S$ SBs per site. The quartic Hamiltonian is expressed in terms of products of SU(2) invariant bond operators that explicitly preserve the rotational invariance of the Heisenberg interaction. Magnetic ordering manifests in this formalism via condensation of the SBs [2–5]. Historically, the SBT was motivated by multiple

reasons: (i) the mean-field decoupling or saddle-point (SP) expansion preserves the SU(2) symmetry, implying that this approach does not violate Mermin-Wagner’s theorem [6]; (ii) unfrustrated and highly frustrated Heisenberg models can be studied with the same formalism, which is suitable for describing both spin liquid and magnetically ordered states; (iii) fractional excitations of spin liquid states, known as *spinons*, become single-particle excitations coupled to an emergent gauge field; and (iv) it can be formulated as a large- N (number of flavors of the SBs) theory, implying that observables can be expanded in powers of $1/N$. The widespread use of the SBT [1,7–39] over the past 30 years is a natural consequence of its versatility. However, during the past two decades, the interest has mainly focused on quantum spin liquids [24,39–66] and their classification by means of the projective symmetry group theory [25,32,34,36,39–41,60,67].

In general, most attempts at using the SBT for describing magnetically ordered and spin liquid states have not gone beyond the saddle-point (SP) level. As we will see in this work, this situation could be a natural consequence of several subtleties that have been omitted in previous formulations of the theory and that become particularly important for studying the excitation spectrum of magnetically ordered (or condensed) states. The increasing need to make progress on this front is manifested by a number of magnetically ordered triangular antiferromagnets, such as $\text{Ba}_3\text{CoSb}_2\text{O}_9$ [68–73], whose inelastic neutron scattering cross section cannot be explained with a large- S expansion due to their proximity to a “quantum melting point” [70,73].

Motivated by these experimental results, we initiated a zero-temperature study of the $1/N$ corrections of the dynamical spin structure factor of the triangular Heisenberg model. A proper treatment of the condensed phase— 120° Néel state—revealed several technical subtleties that have led to misleading interpretations of the SP results and to apparent failures of the SBT [37,38,74]. The most outstanding misinterpretation is the identification of the collective modes with the poles of the dynamical spin structure factor that is obtained at the SP level. We note that these poles coincide with the single-spinon dispersion of the SBT, which in general does not coincide with the single-magnon dispersion. As we have explained in previous works [37,38], the inclusion of an additional diagram that would be of order $1/N$ in the absence of the condensate leads to an exact cancellation of the SP poles and to the emergence of new poles (zeros of the fluctuation matrix) that represent the true collective modes (magnons) of the system. The correct identification of the true collective modes allowed us to recover the linear SWT result by taking the large- S limit of the SBT [38]. This identification also explains the failed attempts at recovering the correct large- S limit at the SP level of the SBT [75,76]. Unfortunately, this negative result was misinterpreted as an important shortcoming of the SBT that discouraged the use of this formalism for modeling the excitation spectrum of ordered magnets.

The above-mentioned results have stimulated us to revisit the simpler case of the square Heisenberg model, where the absence of frustration leads to collinear antiferromagnetic ordering at $T = 0$ [2,7]. What are our motivations to revisit this old problem? Our first motivation is to understand the differences between different SP approximations that can be used to describe *the same* magnetically ordered state. This freedom is not only related to different ways of decoupling the Heisenberg Hamiltonian into products of two bond operators, but also to the choice of the condensate for a particular decoupling scheme. As we will see in this work, the differences between different decoupling schemes parametrized by the continuous parameter α become less important upon including higher-order corrections in $1/N$. In particular, we will see that the dynamical spin structure factor coincides with the linear spin wave result in the $S \rightarrow \infty$ limit *for any value of α* . As for the choice of the condensate, we will see that different condensates that describe the same long-range magnetic ordering lead to different low-order $1/N$ corrections of the dynamical spin susceptibility. Correspondingly, at the SP level, there is an optimal choice of the condensate that can be continuously connected with the *simple* Bose-Einstein condensate (BEC) solution (all bosons are condensed in the same mode) [77] obtained for noncollinear orderings (the square lattice can be continuously deformed into a triangular lattice).

The second important motivation is to revisit the diagrammatic $1/N$ expansion [2,7] in the presence of a condensate. In particular, we will demonstrate that each Feynman diagram of the dynamical spin susceptibility $\chi(\mathbf{k}, \omega)$ has contributions of different order in $1/N$ in the presence of a condensate. More importantly, this mixed character of each Feynman diagram leads to an exact cancellation of the single-spinon poles to any order in $1/N$. In other words, for each diagram that includes single-spinon poles, there is a counterdiagram that removes

these spurious poles from the excitation spectrum of a magnetically ordered state. Since the *noncondensed* parts of the diagram and the counterdiagram are of different order in $1/N$, this result forced us to reconsider the diagrammatic hierarchy in the presence of a condensate: for each diagram that is included in the calculation, one must also include the corresponding counterdiagram to obtain physically correct results. In particular, this explains why the SP result is in general not enough to obtain a qualitatively correct dynamical spin structure factor. From a technical point of view, we uncover the unusual structure of the $1/N$ diagrammatic expansion of the dynamical spin susceptibility in the condensed phase. Namely, diagrams of $\chi_{\text{FL}}(\mathbf{k}, \omega)$ that are nominally of order $1/N$ and account for the fluctuations around the SP solution include a singular contribution of order $O(1/N^0)$ whenever the condensate fraction is finite. This contribution corresponds to isolated poles with residues of order $O(1/N^0)$ that exactly cancel the single-spinon poles of the saddle-point solution $\chi_{\text{SP}}(\mathbf{k}, \omega)$. In general, for each diagram we identify the counterdiagram that must be included to cancel the unphysical single-spinon poles.

The article is organized as follows. In Sec. II we introduce the SB representation of the Heisenberg model along with its generalization to an arbitrary number N of bosonic flavors. We also introduce the most general decoupling scheme of the spin Hamiltonian in terms of products of bond operators. Section III is devoted to the path integral formulation based on the Hubbard-Stratonovich transformation associated with the bond operator decoupling described in Sec. II. The SP approximation and the corresponding SP solution (spinon condensation associated with long-range magnetic ordering) are discussed in Sec. IV. This section also includes a discussion of the different ways in which the SBs can be condensed in the thermodynamic limit. In Sec. V we introduce the formalism required to go beyond the SP level, and in Sec. VI we demonstrate the nontrivial cancellation of the single-spinon poles of the dynamical spin structure factor. In particular, Sec. VI includes a careful derivation of the diagrammatic expansion in the presence of a condensate. The emergence of the true collective modes (magnons) of the theory is presented in Sec. VII. This section also includes a comparison between the results that are obtained for different values of α . The main results of the manuscript are summarized in Sec. VIII.

II. SCHWINGER BOSON REPRESENTATION

We will consider the antiferromagnetic (AFM) Heisenberg model

$$\hat{H}_{\text{AFM}} = \sum_{\langle i,j \rangle} J_{ij} \hat{\mathcal{S}}_i \cdot \hat{\mathcal{S}}_j, \quad (1)$$

where $\hat{\mathcal{S}}_i$ is the spin operator at the lattice site i , and $J_{ij} > 0$ is the antiferromagnetic exchange constant. For a bipartite lattice [7–9], this Hamiltonian can be generalized by replacing the spin operators, which are generators of the SU(2) group, with the generators of the SU(N) group. For the generalization of the AFM Heisenberg model, we must use conjugate representations of SU(N) for each of the two A and B sublattices [78]. In terms of an N -component Schwinger boson, $\hat{b}_i = (\hat{b}_{i,1}, \dots, \hat{b}_{i,N})^T$, the generators of the SU(N)

group can be expressed as $\hat{S}_i^{mn} = \hat{b}_{i,m}^\dagger \hat{b}_{i,n}$ on the A sublattice and $\hat{S}_i^{mn} = \hat{b}_{i,n}^\dagger \hat{b}_{i,m}$ on the B sublattice [2,7,8]. The constraint equation

$$\sum_m \hat{b}_{i,m}^\dagger \hat{b}_{i,m} = NS, \quad (2)$$

where NS is an integer number, determines a particular representation of $SU(N)$. In other words, S represents the spin size for $N = 2$.

Because of the requirement of conjugate representations for the two different sublattices, this $SU(N)$ extension does not apply to Heisenberg antiferromagnets on nonbipartite lattices. A more ‘‘flexible’’ generalization of the spin operator is provided by the generators of the $Sp(N/2)$ group, for even values of N , because all spin operators belong to the same representation [11]. The corresponding generalization of the AFM Heisenberg Hamiltonian is

$$\hat{H}_{Sp(N/2)} = \sum_{(i,j)} \frac{4J_{ij}}{N} \left(\frac{NS^2}{4} - \hat{A}_{ij}^\dagger \hat{A}_{ij} \right). \quad (3)$$

The operator

$$\hat{A}_{ij}^\dagger = \frac{1}{2} \sum_{\sigma=-N/2}^{N/2} \text{sgn}(\sigma) \hat{b}_{i\bar{\sigma}}^\dagger \hat{b}_{j\sigma}^\dagger, \quad (4)$$

with $\bar{\sigma} = -\sigma$, creates a singlet state that is invariant under the group of $Sp(N/2)$ transformations.

There is still another generalization of the AFM Heisenberg model based on the so-called ‘‘symplectic spin’’ [28], which preserves the odd nature of the spin operator under time-reversal transformation. The generalized spin operators generate a subgroup of $SU(N)$, dubbed as $Sy(N/2)$ in this work. The corresponding Hamiltonian is

$$\hat{H}_{Sy(N/2)} = \sum_{(i,j)} \frac{2J_{ij}}{N} (: \hat{B}_{ij}^\dagger \hat{B}_{ij} : - \hat{A}_{ij}^\dagger \hat{A}_{ij}), \quad (5)$$

where the bond operator \hat{A}_{ij}^\dagger has been defined in Eq. (4) and

$$\hat{B}_{ij}^\dagger = \frac{1}{2} \sum_{\sigma=-N/2}^{N/2} \hat{b}_{i\sigma}^\dagger \hat{b}_{j\sigma}^\dagger. \quad (6)$$

Although these generalizations of the AFM Heisenberg model are different for $N > 2$, they coincide for the physical case of interest ($N = 2$) because $Sp(1)$ and $Sy(1)$ are isomorphic to $SU(2)$. The following identity holds for this particular ($N = 2$) case:

$$: \hat{B}_{ij}^\dagger \hat{B}_{ij} : + \hat{A}_{ij}^\dagger \hat{A}_{ij} = S^2. \quad (7)$$

This identity allows us to express the $N = 2$ AFM Heisenberg Hamiltonian in multiple ways that are parametrized by the continuous parameter α :

$$\hat{H}_{SB}(\alpha, N) = \sum_{(i,j)} \frac{4J_{ij}}{N} [C_\alpha + \alpha : \hat{B}_{ij}^\dagger \hat{B}_{ij} : - (1 - \alpha) \hat{A}_{ij}^\dagger \hat{A}_{ij}], \quad (8)$$

where $C_\alpha = NS^2(1/4 - \alpha/2)$. In other words, $\hat{H}_{SB}(\alpha, N = 2)$ is independent of α up to an irrelevant additive constant. As we will see in this work, while the different mean-field decouplings of \hat{H}_{SB} associated with each value of the continuous

parameter α lead to very different SP solutions, the inclusion of a $1/N$ correction makes the dynamical spin structure factor (DSSF) much less dependent on α . In particular, we will demonstrate that the DSSF coincides with the linear spin wave result in the large- S limit for any value of α .

For concreteness, we will focus on the square lattice. As we will see later, the collinear nature of the AFM ordering in this lattice introduces more freedom in the choice of the spinon condensate. The rest of the analysis, which is included in the next sections, can be extended to other lattices/models, including nonbipartite lattices with noncollinear magnetic orderings.

III. PATH-INTEGRAL FORMULATION

Equation (8) provides a natural decoupling scheme to perform the Hubbard-Stratonovich transformation that is the basis of the SBT. As we already mentioned, due to the singlet character of the bond operators \hat{A}_{ij} and \hat{B}_{ij} , the SP equations, or equivalently the mean-field Hamiltonian, produced by this decoupling scheme do not explicitly break the $SU(2)$ symmetry of the Heisenberg Hamiltonian. The basic steps for implementing the path integral over coherent states can be found in Refs. [2,79].

After performing the Hubbard-Stratonovich transformation, the partition function of the model Hamiltonian Eq. (8) can be expressed as the path integral [37]

$$\mathcal{Z} = \int \mathcal{D}[\bar{W}W\lambda] \int \mathcal{D}[\bar{b}b] \exp(-NS(\bar{W}, W, \lambda, \bar{b}, b)). \quad (9)$$

\bar{W}, W are the Hubbard-Stratonovich (HS) complex fields, b is the complex field of eigenvalues of the annihilation SB operators \hat{b} (the corresponding eigenkets are coherent states), and λ is a real field introduced to enforce the constraint Eq. (2). The action $S(\bar{W}, W, \lambda, \bar{b}, b)$ can be decomposed into three terms:

$$S(\bar{W}, W, \lambda, \bar{b}, b) = S_0(\bar{W}, W, \lambda) + S_{b\lambda}(\bar{b}, b, \lambda) + S_{bW}(\bar{b}, b, \bar{W}, W), \quad (10)$$

with

$$S_0(\bar{W}, W, \lambda) = \int_0^\beta d\tau \sum_{(ij)} \frac{1}{4J_{ij}} [\alpha \bar{W}_{ij}^B(\tau) W_{ij}^B(\tau) + (1 - \alpha) \bar{W}_{ij}^A(\tau) W_{ij}^A(\tau)] - iS \int_0^\beta d\tau \sum_i \lambda_i(\tau), \quad (11)$$

$$S_{b\lambda}(\bar{b}, b, \lambda) = \frac{1}{2N} \int_0^\beta d\tau \sum_i \psi_i^\dagger (\partial_\tau \gamma^0 + i\lambda_i(\tau)) \psi_i, \quad (12)$$

$$S_{bW}(\bar{b}, b, \bar{W}, W) = \frac{\alpha}{N} \int_0^\beta d\tau \sum_{(ij)} [\psi_i^\dagger (\Gamma_B \bar{W}_{ji}^B - \Gamma_B^\dagger W_{ij}^B) \psi_j] - \frac{1 - \alpha}{N} \int_0^\beta d\tau \sum_{(ij)} [\psi_i^\dagger (\Gamma_A \bar{W}_{ji}^A + \Gamma_A^\dagger W_{ij}^A) \psi_j], \quad (13)$$

where β is the inverse temperature, $\psi_i^\dagger = (\bar{b}_{i,N/2}, \dots, \bar{b}_{i,-N/2}, b_{i,N/2}, \dots, b_{i,-N/2})$ is the $2N$ -component

Nambu-spinor, the superindex μ of \bar{W}_{ij}^μ and W_{ij}^μ denotes the auxiliary field that decouples the $\bar{A}_{ij}A_{ij}$ and $\bar{B}_{ij}B_{ij}$ terms of the Hamiltonian Eq. (8), and λ_i is a Lagrange multiplier that enforces the local constraint Eq. (2) on each site. The constant matrix γ^0 is defined by $\gamma^0 \equiv \sigma_z \otimes I_0$, where I_0 is the $N \times N$ identity matrix. The bond fields can be expressed in terms of the Nambu-spinor as

$$A_{ij} = \psi_j^\dagger \Gamma_A \psi_i, \quad B_{ij} = \psi_j^\dagger \Gamma_B \psi_i, \quad (14)$$

where Γ_A and Γ_B are the matrices of the bilinear forms given in Eqs. (4) and (6), respectively.

The Nambu representation has an artificial ‘‘particle-hole’’ symmetry because $\psi_i = P(\psi_i^\dagger)^T$, where $P = \sigma_x \otimes I_0$. We can then rewrite the bond fields in the more symmetric form

$$B_{ij} = \frac{1}{2} \psi_j^\dagger \Gamma_B \psi_i + \frac{1}{2} \psi_i^\dagger \Upsilon_B \psi_j, \quad (15)$$

$$A_{ij} = \frac{1}{2} \psi_j^\dagger \Gamma_A \psi_i + \frac{1}{2} \psi_i^\dagger \Upsilon_A \psi_j, \quad (16)$$

where $\Upsilon_B = P\Gamma_B^T P$ and $\Upsilon_A = P\Gamma_A^T P$. The effective action (10) is invariant under the U(1) gauge transformation $b_{i\alpha}(\tau) \rightarrow b_{i\alpha}(\tau)e^{i\theta_i(\tau)}$ if the auxiliary fields transform as

$$\begin{aligned} W_{ij}^\mu(\tau) &\rightarrow W_{ij}^\mu(\tau)e^{i(\theta_i(\tau) \pm \theta_j(\tau))}, \\ \bar{W}_{ij}^\mu(\tau) &\rightarrow \bar{W}_{ij}^\mu(\tau)e^{-i(\theta_i(\tau) \pm \theta_j(\tau))}, \\ \lambda_i(\tau) &\rightarrow \lambda_i(\tau) - \partial_\tau \theta_i(\tau), \end{aligned} \quad (17)$$

where the + and – signs hold for $\mu = A$ and B , respectively.

The momentum space representation of the action is obtained by Fourier transforming the fields

$$\psi_i^\dagger(\tau) = \frac{1}{\sqrt{\mathcal{N}_s \beta}} \sum_{\mathbf{k}, i\omega_n} \psi^\dagger(\mathbf{k}, i\omega_n) C_1(i\omega_n) e^{-i(\mathbf{k}\cdot\mathbf{r}_i - \omega_n \tau)}, \quad (18)$$

$$\psi_i(\tau) = \frac{1}{\sqrt{\mathcal{N}_s \beta}} \sum_{\mathbf{k}, i\omega_n} C_2(i\omega_n) \psi(\mathbf{k}, i\omega_n) e^{i(\mathbf{k}\cdot\mathbf{r}_i - \omega_n \tau)}, \quad (19)$$

$$W_{i,i+\delta}^\mu(\tau) = \frac{1}{\sqrt{\mathcal{N}_s \beta}} \sum_{\mathbf{k}, i\omega_n} e^{i(\mathbf{k}\cdot\mathbf{r}_i - \omega_n \tau)} W_\delta^\mu(\mathbf{k}, i\omega_n), \quad (20)$$

$$\bar{W}_{i,i+\delta}^\mu(\tau) = \frac{1}{\sqrt{\mathcal{N}_s \beta}} \sum_{\mathbf{k}, i\omega_n} e^{-i(\mathbf{k}\cdot\mathbf{r}_i - \omega_n \tau)} \bar{W}_\delta^\mu(\mathbf{k}, i\omega_n), \quad (21)$$

$$\lambda_i(\tau) = \frac{1}{\sqrt{\mathcal{N}_s \beta}} \sum_{\mathbf{k}, i\omega_n} e^{i(\mathbf{k}\cdot\mathbf{r}_i - \omega_n \tau)} \lambda(\mathbf{k}, i\omega_n), \quad (22)$$

where \mathcal{N}_s is the number of lattice sites. The lattice sites have been labeled by the position vector \mathbf{r}_i , and δ is the relative vector connecting neighboring sites. The matrices

$$C_1(i\omega_n) = \begin{pmatrix} I_0 e^{i\omega_n \eta^+} & 0 \\ 0 & I_0 \end{pmatrix}, \quad C_2(i\omega_n) = \begin{pmatrix} I_0 & 0 \\ 0 & I_0 e^{-i\omega_n \eta^+} \end{pmatrix}$$

include the convergence factors required to ensure the normal ordering of the spinor fields \bar{b} , b in the action. The resulting expression of the action is

$$S(\bar{W}, W, \lambda, \bar{b}, b) = -iS\sqrt{\mathcal{N}_s \beta} \lambda(\mathbf{0}, i0) + \sum_{\delta > \mathbf{0}} \frac{1}{4J_\delta} \sum_k [\alpha \bar{W}_\delta^B(k) W_\delta^B(k) + (1 - \alpha) \bar{W}_\delta^A(k) W_\delta^A(k)] + \frac{1}{2N} \sum_{k,p} \psi^\dagger(k) \mathcal{M}(k; p) \psi(p), \quad (23)$$

where $k \equiv (\mathbf{k}, i\omega_n)$, $p \equiv (\mathbf{p}, i\nu_m)$, the sum $\delta > \mathbf{0}$ runs over all translation-nonequivalent bonds, and the dynamical matrix

$$\begin{aligned} \mathcal{M}(k; p) &= -i\omega_n C_1(i\omega_n) \gamma^0 C_2(i\omega_n) \delta_{k,p} + \frac{1}{\sqrt{\mathcal{N}_s \beta}} v_\lambda(k; p) \lambda(k - p) \\ &+ \frac{1}{\sqrt{\mathcal{N}_s \beta}} \sum_{\delta > \mathbf{0}} [v_{W_\delta^B}(k; p) W_\delta^B(k - p) + v_{W_\delta^A}(k; p) W_\delta^A(k - p)] \\ &+ \frac{1}{\sqrt{\mathcal{N}_s \beta}} \sum_{\delta > \mathbf{0}} [v_{\bar{W}_\delta^B}(k; p) \bar{W}_\delta^B(p - k) + v_{\bar{W}_\delta^A}(k; p) \bar{W}_\delta^A(p - k)] \end{aligned} \quad (24)$$

has been expressed in terms of the internal vertices

$$\begin{aligned} v_{W_\delta^A}(k; p) &= \left(\frac{1}{\sqrt{\mathcal{N}_s \beta}} \right)^{-1} \frac{\delta \mathcal{M}(k; p)}{\delta W_\delta^A(k - p)} = -(1 - \alpha) C_1(i\omega_n) (\Gamma_A^\dagger e^{i\mathbf{p}\cdot\delta} + \Upsilon_A^\dagger e^{-i\mathbf{k}\cdot\delta}) C_2(i\nu_m), \\ v_{W_\delta^B}(k; p) &= \left(\frac{1}{\sqrt{\mathcal{N}_s \beta}} \right)^{-1} \frac{\delta \mathcal{M}(k; p)}{\delta W_\delta^B(k - p)} = -\alpha C_1(i\omega_n) (\Gamma_B^\dagger e^{i\mathbf{p}\cdot\delta} + \Upsilon_B^\dagger e^{-i\mathbf{k}\cdot\delta}) C_2(i\nu_m), \\ v_{\bar{W}_\delta^A}(k; p) &= \left(\frac{1}{\sqrt{\mathcal{N}_s \beta}} \right)^{-1} \frac{\delta \mathcal{M}(k; p)}{\delta \bar{W}_\delta^A(p - k)} = -(1 - \alpha) C_1(i\omega_n) (\Gamma_A e^{-i\mathbf{k}\cdot\delta} + \Upsilon_A e^{i\mathbf{p}\cdot\delta}) C_2(i\nu_m), \\ v_{\bar{W}_\delta^B}(k; p) &= \left(\frac{1}{\sqrt{\mathcal{N}_s \beta}} \right)^{-1} \frac{\delta \mathcal{M}(k; p)}{\delta \bar{W}_\delta^B(p - k)} = \alpha C_1(i\omega_n) (\Gamma_B e^{-i\mathbf{k}\cdot\delta} + \Upsilon_B e^{i\mathbf{p}\cdot\delta}) C_2(i\nu_m), \\ v_\lambda(k; p) &= \left(\frac{1}{\sqrt{\mathcal{N}_s \beta}} \right)^{-1} \frac{\delta \mathcal{M}(k; p)}{\delta \lambda(k - p)} = iC_1(i\omega_n) C_2(i\nu_m). \end{aligned} \quad (25)$$

The bosonic field can be integrated out to obtain an effective action in terms of the auxiliary fields \bar{W} , W , and λ :

$$\mathcal{Z} = \int \mathcal{D}[\bar{W}W\lambda] \exp(-NS_{\text{eff}}(\bar{W}, W, \lambda)), \quad (26)$$

where

$$S_{\text{eff}}(\bar{W}, W, \lambda) = S_0[\bar{W}, W, \lambda] + \frac{1}{2N} \text{Tr} \ln(\mathcal{M}). \quad (27)$$

Note that the dynamical matrix \mathcal{M} acts on the space $(\xi, \mathbf{q}, \omega)$, where ξ refers to the index of the Nambu spinor.

Since it is not possible to obtain the exact partition function associated with the action (27), we need to introduce an approximation scheme. As usual in these cases, we expand the action in powers of $1/N$ [38]. The lowest order $O(1/N^0)$ term corresponds to the SP solution, which becomes exact in the $N \rightarrow \infty$ limit. The SP solution for the effective action, $S_{\text{eff}}^{\text{SP}}$, is determined from the saddle-point conditions $\delta S_{\text{eff}}^{\text{SP}}/\delta W_{\delta}^{\mu}(q) = 0$ and $\delta S_{\text{eff}}^{\text{SP}}/\delta \lambda(q) = 0$, which lead to

$$\alpha \bar{W}_{\delta}^B(q)|_{\text{SP}} + \frac{2J_{\delta}}{\sqrt{\mathcal{N}_s\beta}} \sum_p \frac{1}{N} \text{Tr}[\mathcal{G}_{\text{SP}}(p; p+q)v_{W_{\delta}^B}(p+q; p)] = 0, \quad (28)$$

$$(1-\alpha)\bar{W}_{\delta}^A(q)|_{\text{SP}} + \frac{2J_{\delta}}{\sqrt{\mathcal{N}_s\beta}} \sum_p \frac{1}{N} \text{Tr}[\mathcal{G}_{\text{SP}}(p; p+q)v_{W_{\delta}^A}(p+q; p)] = 0, \quad (29)$$

$$iS\delta_{q,0} - \frac{1}{2\mathcal{N}_s\beta} \sum_p \frac{1}{N} \text{Tr}[\mathcal{G}_{\text{SP}}(p; p+q)v_{\lambda}(p+q; p)] = 0, \quad (30)$$

where $q \equiv (\mathbf{q}, i\omega_n)$, $p \equiv (\mathbf{p}, i\nu_m)$, and

$$\mathcal{G}_{\text{SP}}(p; p+q) = \frac{1}{\mathcal{Z}_{\text{SP}}} \int \mathcal{D}[\bar{b}b] e^{-NS_{\text{eff}}(\bar{W}_{\text{SP}}, W_{\text{SP}}, \lambda_{\text{SP}}, \bar{b}, b)} \psi(p)\psi^{\dagger}(p+q) \quad (31)$$

is the Schwinger boson's Green's function, and $\mathcal{Z}_{\text{SP}} = \int \mathcal{D}[\bar{b}b] e^{-NS_{\text{eff}}(\bar{W}_{\text{SP}}, W_{\text{SP}}, \lambda_{\text{SP}}, \bar{b}, b)}$.

IV. SADDLE-POINT APPROXIMATION AND SPINON CONDENSATION

The next step is to solve the self-consistent SP equations [Eqs. (28)–(30)]. As we will see in this section, the magnetic ordering of the ground state manifests via the condensation of the SBs in a single-particle ground state (zero-energy single-spinon mode). The existence of multiple zero-energy single-spinon modes introduces some freedom in the selection of the single-spinon BEC. Part of this freedom is associated with the possible orientations of the staggered magnetization (order parameter), and it is removed by the inclusion of an infinitesimal staggered magnetic field h that is sent to zero at the end of the calculation. However, for collinear magnetic orderings there is still some remaining freedom associated with the existence of two zero modes with a given spin polarization. As we will see later, all of these condensates describe the same type of collinear magnetic ordering, and the choice of a ‘‘simple BEC’’ (condensation in a unique single-spinon mode) becomes advantageous upon adding corrections beyond the SP approximation.

For concreteness, we will consider the square lattice antiferromagnet ($N = 2$) with C_4 symmetry ($J_{\delta} \equiv J$) and the general decomposition of the spin Hamiltonian given in Eq. (8). Since the ground state of the square lattice AFM Heisenberg model exhibits Néel antiferromagnetic order, it is convenient to work in a twisted reference frame, $\hat{\mathbf{S}}'_{i \in A} = \hat{\mathbf{S}}_{i \in A}$ and $\hat{\mathbf{S}}'_{i \in B} = (-\hat{S}_i^x, \hat{S}_i^y, -\hat{S}_i^z)$, where the magnetic order becomes ferromagnetic. Going back to the canonical formalism,

the Schwinger boson spinors in the original and new reference frames are

$$\hat{\mathbf{b}}_j = \begin{pmatrix} \hat{b}_{j,\uparrow} \\ \hat{b}_{j,\downarrow} \end{pmatrix}, \quad \hat{\mathbf{b}}'_j = \begin{pmatrix} \hat{b}'_{j,\uparrow} \\ \hat{b}'_{j,\downarrow} \end{pmatrix}, \quad (32)$$

respectively. These two spinors are related by the transformation

$$\hat{\mathbf{b}}'_j = \hat{\mathbf{b}}_j \quad \text{for } j \in A, \quad \hat{\mathbf{b}}'_j = e^{i\frac{\pi}{2}\sigma_y} \hat{\mathbf{b}}_j \quad \text{for } j \in B, \quad (33)$$

which leads to the following transformation of the bond operators:

$$\hat{A}_{ij} = e^{i\pi \cdot r_i} \hat{A}'_{ij}, \quad \hat{B}_{ij} = e^{i\pi \cdot r_i} \hat{B}'_{ij}, \quad (34)$$

where $\boldsymbol{\pi} = (\pi, \pi)$ and

$$\hat{A}'_{ij} = -(1/2)\hat{\mathbf{b}}_i^{\dagger}(\hat{\mathbf{b}}_j^{\dagger})^T, \quad \hat{B}'_{ij} = (1/2)\hat{\mathbf{b}}_j^{\dagger}(i\sigma^y)\hat{\mathbf{b}}_i. \quad (35)$$

The generalization of the transformation in Eq. (33) to arbitrary values of N is

$$\hat{b}'_{j\sigma} = \hat{b}_{j\sigma} \quad \text{for } j \in A, \quad \hat{b}'_{j\sigma} = \text{sgn}(\sigma)\hat{b}_{j\bar{\sigma}} \quad \text{for } j \in B. \quad (36)$$

From now on we will work in the twisted frame, and the *prime* will be dropped to simplify the notation.

Knowing that the ground-state ordering corresponds to a uniform ferromagnetic solution in the twisted reference frame, the SP solution of interest must be *uniform and static*. From the projective symmetry group analysis [34], uniform ferromagnetic order (twisted reference frame) can be obtained via spinon condensation in the 0-flux phase defined by the SP

solution

$$W_{\delta}^B|_{\text{SP}} = -(\bar{W}_{\delta}^B|_{\text{SP}})^* = -2J\mathcal{B}_{\delta}, \quad (37)$$

$$W_{\delta}^A|_{\text{SP}} = (\bar{W}_{\delta}^A|_{\text{SP}})^* = 2J\mathcal{A}_{\delta}, \quad (38)$$

$$\lambda_r(\tau)|_{\text{SP}} = -i\lambda, \quad (39)$$

with

$$\mathcal{A}_{(1,0)} = \mathcal{A}_{(0,1)} = A_x, \quad (40)$$

$$\mathcal{B}_{(1,0)} = -\mathcal{B}_{(0,1)} = iB_x, \quad (41)$$

where A_x , B_x , and λ are real numbers. The uniform and static character of the SP solution makes the dynamical matrix diagonal in momentum and frequency space, $\mathcal{M}(k; q) = \mathcal{M}(q)\delta_{k,q}$, where

$$\mathcal{M}(q) = \frac{1}{2}C_1(i\omega_n)[-i\omega_n\gamma^0 + H_{\text{sp}}(\mathbf{q})]C_2(i\omega_n), \quad (42)$$

and

$$H_{\text{sp}}(\mathbf{q}) = \begin{pmatrix} \lambda & -i\xi_q & \Delta_q & 0 \\ i\xi_q & \lambda & 0 & \Delta_q \\ \Delta_q & 0 & \lambda & i\xi_q \\ 0 & \Delta_q & -i\xi_q & \lambda \end{pmatrix} \quad (43)$$

is the SP Hamiltonian matrix. The operator

$$\hat{H}_{\text{SP}} = \sum_{\mathbf{q}} \hat{\psi}^{\dagger}(\mathbf{q})H_{\text{sp}}(\mathbf{q})\hat{\psi}(\mathbf{q}) \quad (44)$$

is the corresponding Hamiltonian in momentum space, where

$$\hat{\psi}(\mathbf{q}) = \frac{1}{\sqrt{\mathcal{N}_s}} \sum_j \hat{\psi}_j e^{i\mathbf{q}\cdot\mathbf{r}_j} \quad (45)$$

is the Fourier transform of the Nambu-spinor operator

$$\hat{\psi}_j = \begin{pmatrix} \hat{b}_{j\uparrow} \\ \hat{b}_{j\downarrow} \\ \hat{b}_{j\uparrow}^{\dagger} \\ \hat{b}_{j\downarrow}^{\dagger} \end{pmatrix}. \quad (46)$$

The matrix elements of $H_{\text{sp}}(\mathbf{q})$ are

$$\Delta_q = 2(1 - \alpha)JA_x\gamma_q^+, \quad \xi_q = 8\alpha JB_x\gamma_q^-, \quad (47)$$

and $\gamma_q^{\pm} = \frac{1}{2}(\cos q_x \pm \cos q_y)$.

A. Symmetry analysis

The bond operators \hat{A}_{ij} and \hat{B}_{ij} are both invariant under global SU(2) spin rotations $\mathcal{U}_n(\varphi)$ in the original reference frame. In the twisted reference frame, this SU(2) symmetry group is generated by *staggered* U(1) spin rotations, \mathcal{U}'_x and \mathcal{U}'_z , about the x and z axes, and by a *uniform* U(1) spin rotation \mathcal{U}'_y about the y axis. The transformation rules of the Schwinger bosons under these symmetry operations read

$$\mathcal{U}'_x(\varphi)\hat{\mathbf{b}}_j\mathcal{U}'_x{}^{\dagger}(\varphi) = e^{-i\eta_j\frac{\varphi}{2}\sigma_x}\hat{\mathbf{b}}_j, \quad (48)$$

$$\mathcal{U}'_y(\varphi)\hat{\mathbf{b}}_j\mathcal{U}'_y{}^{\dagger}(\varphi) = e^{-i\frac{\varphi}{2}\sigma_y}\hat{\mathbf{b}}_j, \quad (49)$$

$$\mathcal{U}'_z(\varphi)\hat{\mathbf{b}}_j\mathcal{U}'_z{}^{\dagger}(\varphi) = e^{-i\eta_j\frac{\varphi}{2}\sigma_z}\hat{\mathbf{b}}_j, \quad (50)$$

where $\eta_j = +1$ (-1) on the A (B) sublattice. In momentum space, these transformations become

$$\mathcal{U}'_x(\varphi)\hat{\mathbf{b}}_q\mathcal{U}'_x{}^{\dagger}(\varphi) = \cos\frac{\varphi}{2}\hat{\mathbf{b}}_q - i\sin\frac{\varphi}{2}\sigma_x\hat{\mathbf{b}}_{q+\pi}, \quad (51)$$

$$\mathcal{U}'_y(\varphi)\hat{\mathbf{b}}_q\mathcal{U}'_y{}^{\dagger}(\varphi) = e^{-i\frac{\varphi}{2}\sigma_y}\hat{\mathbf{b}}_q, \quad (52)$$

$$\mathcal{U}'_z(\varphi)\hat{\mathbf{b}}_q\mathcal{U}'_z{}^{\dagger}(\varphi) = \cos\frac{\varphi}{2}\hat{\mathbf{b}}_q - i\sin\frac{\varphi}{2}\sigma_z\hat{\mathbf{b}}_{q+\pi}. \quad (53)$$

The SP Hamiltonian remains invariant under these transformations because the bond operators \hat{A}_{ij} and \hat{B}_{ij} are SU(2) invariants. By taking $\varphi = \pi$, we obtain

$$w_{\mu}^{\dagger}H_{\text{sp}}(\mathbf{q})w_{\mu} = H_{\text{sp}}(\mathbf{q} + \boldsymbol{\pi}) \quad \text{for } \mu = x, z, \quad (54)$$

$$w_y^{\dagger}H_{\text{sp}}(\mathbf{q})w_y = H_{\text{sp}}(\mathbf{q}), \quad (55)$$

where $w_{\mu} = -i\sigma_z \otimes \sigma_{\mu}$ and $w_y = -i\sigma_0 \otimes \sigma_y$ are the matrices associated with the π -rotations of the Nambu spinor Eq. (46) along the μ and y axis. After the para-unitary diagonalization [80], the spectrum of the SP Hamiltonian is determined by the eigenvalue equations

$$\gamma^0 H_{\text{sp}}(\mathbf{q})X_{q\sigma} = \varepsilon_{q\sigma}X_{q\sigma}, \quad \gamma^0 H_{\text{sp}}(\mathbf{q})\bar{X}_{q\sigma} = -\varepsilon_{-q\sigma}\bar{X}_{q\sigma}. \quad (56)$$

Equation (54) implies that $\varepsilon_{q\sigma} = \varepsilon_{q+\pi\sigma}$ and $X_{q\sigma} = w_{x/z}X_{q+\pi\sigma}$. In addition, Eq. (55) implies that the eigenstates of $H_{\text{sp}}(\mathbf{q})$ are also eigenstates of w_y : $w_y X_{q\sigma} = \pm iX_{q\sigma}$ because $w_y^2 = -I$. The same symmetry argument holds for the eigenstates with negative eigenvalues.

While a nonzero expectation value of the bond operator \hat{B}_{ij} is allowed by the symmetries of the SP Hamiltonian, this expectation value turns out to be zero because of a cancellation between matrix elements. For instance, in the SP approximation,

$$B_x = (1/2) \sum_{\sigma\mathbf{q}} [\bar{X}_{q\sigma}^{\dagger} i w_y \bar{X}_{q\sigma} (1 + n_B(\varepsilon_{q\sigma})) + X_{q\sigma}^{\dagger} i w_y X_{q\sigma} n_B(\varepsilon_{q\sigma})], \quad (57)$$

where $n_B(\varepsilon)$ is the Bose distribution function. Since $\{w_y, w_z\} = 0$, $\bar{X}_{q\sigma}$ and $\bar{X}_{q+\pi\sigma}$, or $X_{q\sigma}$ and $X_{q+\pi\sigma}$, must be the eigenvectors of w_y with opposite eigenvalues. The relation $X_{q\sigma} = w_{x/z}X_{q+\pi\sigma}$ leads to $\bar{X}_{q\sigma}^{\dagger} i w_y \bar{X}_{q\sigma} = -\bar{X}_{q+\pi\sigma}^{\dagger} i w_y \bar{X}_{q+\pi\sigma}$ and $X_{q\sigma}^{\dagger} i w_y X_{q\sigma} = -X_{q+\pi\sigma}^{\dagger} i w_y X_{q+\pi\sigma}$. Since the occupation numbers $n_B(\varepsilon_{q\sigma})$ at \mathbf{q} and $\mathbf{q} + \boldsymbol{\pi}$ are the same because $\varepsilon_{q\sigma} = \varepsilon_{q+\pi\sigma}$, we obtain $B_x = 0$ at any finite temperature T . As we will show later, at $T = 0$ spinons can condense in multiple ways with different macroscopic occupation numbers of the single-spinon states at $\mathbf{q} = \mathbf{0} \equiv (0, 0)$ and $\boldsymbol{\pi} \equiv (\pi, \pi)$. Nevertheless, we have verified that B_x remains equal to zero for any of these alternative SP solutions. Consequently, the general

SP solutions that we will consider here are described by the bond field \mathcal{A}_δ , which is invariant under a staggered gauge transformation

$$C(\varphi)\hat{\mathbf{b}}_j C^\dagger(\varphi) = e^{-in_j\frac{\varphi}{2}}\hat{\mathbf{b}}_j, \quad (58)$$

or, in momentum space,

$$C(\varphi)\hat{\mathbf{b}}_q C^\dagger(\varphi) = \cos\frac{\varphi}{2}\hat{\mathbf{b}}_q - i\sin\frac{\varphi}{2}\hat{\mathbf{b}}_{q+\pi}. \quad (59)$$

The invariance of the Hamiltonian under gauge transformations restricts the form of the momentum space version of the SP Hamiltonian [see Eq. (44)]. Under the gauge transformation $C(\varphi = \pi)$, the four-dimensional spinor $\psi(\mathbf{q})$ is transformed into $w_0\psi(\mathbf{q} + \boldsymbol{\pi})$ with $w_0 = -i\sigma_z \otimes \sigma_0$. Since $w_0^\dagger H_{\text{sp}}(\mathbf{q})w_0 = H_{\text{sp}}(\mathbf{q} + \boldsymbol{\pi})$, we conclude that $\varepsilon_{q\sigma} = \varepsilon_{q+\pi\sigma}$ and $X_{q\sigma} = w_0 X_{q+\pi\sigma}$.

There is also a ‘‘particle-hole’’ symmetry $PH_{\text{sp}}^*(\mathbf{q})P = H_{\text{sp}}(-\mathbf{q})$ inherited from the Nambu representation. Given that $\{P, \gamma^0\} = 0$, Eq. (56) implies that $P\bar{X}_{q\sigma}^*$ and $PX_{q\sigma}^*$ must be the eigenvectors of $H_{\text{sp}}(-\mathbf{q})$ with eigenenergies $\varepsilon_{-q\sigma}$ and $-\varepsilon_{q\sigma}$, respectively. In the presence of the inversion symmetry, we also have $\varepsilon_{-q\sigma} = \varepsilon_{q\sigma}$.

B. Single-spinon spectrum

Since $\mathcal{B}_\delta = 0$ at the SP level, the SP $SU(2)$ Hamiltonian has two degenerate single-spinon energy branches

$$\varepsilon_{q\sigma} \equiv \varepsilon_q = \sqrt{\lambda^2 - \Delta_q^2}. \quad (60)$$

$\sigma = \pm 1$ represents the spin quantum number, \uparrow, \downarrow , of these spinon modes, whose eigenvectors are

$$X_{q,+1} = \begin{pmatrix} u_q \\ 0 \\ v_q \\ 0 \end{pmatrix}, \quad X_{q,-1} = \begin{pmatrix} 0 \\ u_q \\ 0 \\ v_q \end{pmatrix}, \quad (61)$$

with

$$u_q = \sqrt{\frac{1}{2}\left(\frac{\lambda}{\varepsilon_q} + 1\right)}, \quad v_q = -\frac{\Delta_q}{|\Delta_q|}\sqrt{\frac{1}{2}\left(\frac{\lambda}{\varepsilon_q} - 1\right)}. \quad (62)$$

The corresponding eigenvectors for negative energy eigenvalues, $-\varepsilon_q$, are

$$\bar{X}_{q,+1} = \begin{pmatrix} v_q \\ 0 \\ u_q \\ 0 \end{pmatrix}, \quad \bar{X}_{q,-1} = \begin{pmatrix} 0 \\ v_q \\ 0 \\ u_q \end{pmatrix}. \quad (63)$$

In accordance with Goldstone’s theorem, the spinon condensation leads to a gapless spinon dispersion $\varepsilon_{q\sigma} \equiv \varepsilon_q$ in the thermodynamic limit. The gapless modes have momenta $\mathbf{q} = \mathbf{0}$ and $\boldsymbol{\pi}$, implying that $\lambda = 2(1 - \alpha)JA_x$. The gauge freedom of the theory, $b_{i\sigma}(\tau) \rightarrow b_{i\sigma}(\tau)e^{i\theta_i(\tau)}$, allows us to assume that $A_x > 0$. An explicit solution of the SP equations [Eqs. (28)–(30)] gives at $T = 0$

$$A_x = 2S + c_1, \quad B_x = 0, \quad n_c = 2S - c_2, \quad (64)$$

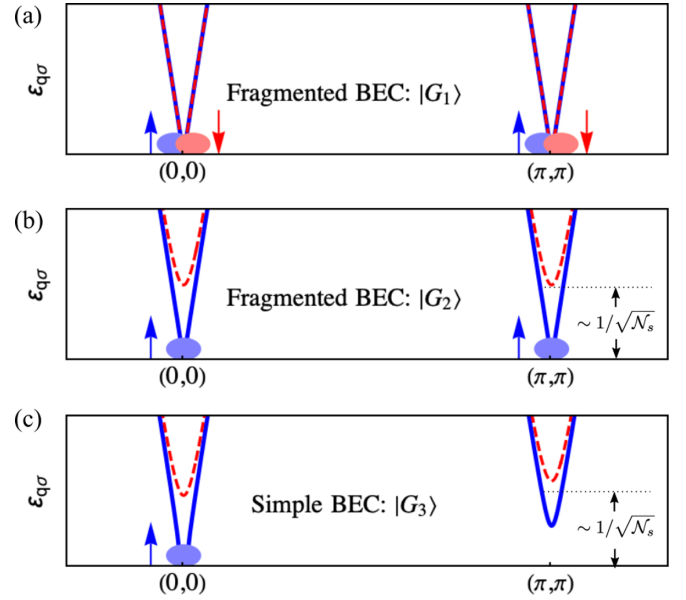


FIG. 1. Single-spinon spectrum of a square lattice antiferromagnet in the absence of a symmetry-breaking field (a), in the presence of a symmetry-breaking field h linearly coupled with the staggered magnetization (b), and with an additional symmetry-breaking field t that couples to a single-spinon nearest-neighbor hopping (c), where $h, t \sim 1/\mathcal{N}_s$.

where

$$c_1 = \int \frac{d^2\mathbf{k}}{(2\pi)^2} (1 - \sqrt{1 - (\gamma_{\mathbf{k}}^+)^2}) \approx 0.158, \quad (65)$$

$$c_2 = \int \frac{d^2\mathbf{k}}{(2\pi)^2} \left(\frac{1}{\sqrt{1 - (\gamma_{\mathbf{k}}^+)^2}} - 1 \right) \approx 0.393, \quad (66)$$

and n_c is the spinon condensate fraction. Since n_c must be positive, the above solution is valid only for $2S > 0.393$, which includes all the physical values of S .

C. Spinon condensation

1. Fragmented versus simple BEC

The above SP Hamiltonian has four zero-energy single-spinon states with $\mathbf{q} = \mathbf{0}$ or $\boldsymbol{\pi}$ and $\sigma = \pm 1$ in the thermodynamic limit, implying that the spinons can condense in multiple ways at zero temperature. We note, however, that this degeneracy is not present on finite-size lattices because the single-spinon spectrum has a finite-size gap that forces the SP solution to be unique and $SU(2)$ -invariant. Consequently, in the absence of any external symmetry-breaking field, the ground state of the SP Hamiltonian remains $SU(2)$ invariant upon taking the thermodynamic limit, implying that spinons condense on the four zero-energy modes with equal condensate fractions:

$$|G_1\rangle = \frac{1}{u_{0\uparrow}^4} e^{-\frac{i\theta_{0\uparrow}^*}{2u_{0\uparrow}^*} \sum_{\sigma} (\hat{b}_{0\sigma}^\dagger \hat{b}_{0\sigma}^\dagger - \hat{b}_{\pi\sigma}^\dagger \hat{b}_{\pi\sigma}^\dagger)} \prod_{\mathbf{k} \neq \mathbf{0}, \boldsymbol{\pi}, \sigma} \frac{1}{u_{k\sigma}} e^{-\frac{i\theta_{k\sigma}^*}{2u_{k\sigma}^*} \hat{b}_{k\sigma}^\dagger \hat{b}_{-k\sigma}^\dagger} |\emptyset\rangle, \quad (67)$$

where $|\emptyset\rangle$ is the vacuum of the Schwinger bosons $b_{i\sigma}$ [see Fig. 1(a)] [81]. The average occupation number n_k of

Schwinger bosons with momentum \mathbf{k} is determined by the ratio $|v_{\mathbf{k}\sigma}/u_{\mathbf{k}\sigma}| = \sqrt{(\lambda - \varepsilon_{\mathbf{k}\sigma})/(\lambda + \varepsilon_{\mathbf{k}\sigma})}$. This ratio satisfies that $\lim_{\mathcal{N}_s \rightarrow \infty} |v_{\mathbf{k}\sigma}/u_{\mathbf{k}\sigma}| \rightarrow 1$ for $\mathbf{k} = \mathbf{0}, \boldsymbol{\pi}$, i.e., at the wave vectors where the spinon spectrum is gapless. The finite-size scaling satisfies $1 - |v_{\mathbf{0}\uparrow}/u_{\mathbf{0}\uparrow}| \propto 1/\mathcal{N}_s$ because the finite-size gap scales as $\varepsilon_{\mathbf{0}\uparrow} \propto 1/\mathcal{N}_s$, implying a macroscopic occupation, $\propto \mathcal{N}_s$, of the four zero-energy single-spinon states. As we will discuss below, this SU(2) invariant spinon condensate corresponds to a ‘‘fragmented’’ BEC [77,82].

As usual, to account for the Néel antiferromagnetic order (in the original reference frame), we must introduce an external symmetry-breaking field h linearly coupled to the staggered magnetization. In the twisted reference frame, this coupling takes the form $-h \sum_{i,\sigma} \sigma \hat{b}_{i\sigma}^\dagger \hat{b}_{i\sigma}$ and the field h is sent to zero after taking the thermodynamic limit. Since the symmetry-breaking field h gaps out the single-spinon branch with spin index \downarrow (the field h is applied along the positive z -direction in the twisted reference frame), the spinons must condense in the remaining two zero-energy states with spin index \uparrow , implying that the ground-state degeneracy is not completely removed [see Fig. 1(b)]. By analogy with the SU(2) invariant solution (67), the bosons still condense in a fragmented BEC,

$$|G_2\rangle = \frac{1}{u_{\mathbf{0}\uparrow}^2} e^{-\frac{v_{\mathbf{0}\uparrow}^*}{2u_{\mathbf{0}\uparrow}^*} (\hat{b}_{\mathbf{0}\uparrow}^\dagger \hat{b}_{\mathbf{0}\uparrow}^\dagger - \hat{b}_{\boldsymbol{\pi}\uparrow}^\dagger \hat{b}_{\boldsymbol{\pi}\uparrow}^\dagger)} \times \prod_{(\mathbf{k},\sigma) \neq (\mathbf{0},\uparrow), (\boldsymbol{\pi},\uparrow)} \frac{1}{u_{\mathbf{k}\sigma}} e^{-\frac{v_{\mathbf{k}\sigma}^*}{2u_{\mathbf{k}\sigma}^*} \hat{b}_{\mathbf{k}\sigma}^\dagger \hat{b}_{-\mathbf{k}\sigma}^\dagger} |\emptyset\rangle, \quad (68)$$

where $1 - |v_{\mathbf{0}\uparrow}/u_{\mathbf{0}\uparrow}| \propto 1/\mathcal{N}_s$ and $1 - |v_{\mathbf{0}\downarrow}/u_{\mathbf{0}\downarrow}| \propto 1/\mathcal{N}_s^\nu$, where $\nu < 1$ is controlled by the finite-size scaling of the symmetry-breaking field. For instance, the finite-size gaps for spin-up and spin-down spinons are $\varepsilon_{\mathbf{0}\uparrow} = \varepsilon_{\boldsymbol{\pi}\uparrow} \propto 1/\mathcal{N}_s$ and $\varepsilon_{\mathbf{0}\downarrow} = \varepsilon_{\boldsymbol{\pi}\downarrow} \propto 1/\mathcal{N}_s^{1/2}$ for a symmetry-breaking field $h \propto 1/\mathcal{N}_s$. In other words, the BEC state Eq. (68) describes a macroscopic occupation of both zero-energy states with spin index up.

We note, however, that previous SB approaches to the square lattice AFM Heisenberg have always adopted the SP solution $|G_2\rangle$ without an explicit justification [2]. In fact, at the SP level, the magnetically ordered state can be equally described by an infinite number of *fragmented* spin condensates with different condensate fractions $(n_{\mathbf{0}}, n_{\boldsymbol{\pi}}) = (n_1, n_c - n_1)$ at the two orthogonal zero-energy modes with $0 < n_1 < n_c$. These condensates are called ‘‘fragmented’’ because the single-particle density matrix has two macroscopic eigenvalues $\mathcal{N}_s n_1$ and $\mathcal{N}_s (n_c - n_1)$. We note that the choice of the two zero-energy modes with different condensate fractions is made by fixing the gauge transformation $C(\varphi)$ introduced in Eq. (59). In particular, the ground state $|G_2\rangle$ corresponds to the gauge choice $\varphi = 0$ and $n_{\mathbf{0}} = n_{\boldsymbol{\pi}} = n_c/2$. Because the two zero modes can be exchanged by applying the gauge transformation $C(\boldsymbol{\pi})$ [see Eq. (59)], the condensate fractions (n_1, n_2) and (n_2, n_1) describe the same physical state.

The ground state of the mean-field Hamiltonian with $n_1 = n_c$, or the gauge equivalent one with $n_2 = n_c$, is called ‘‘simple’’ BEC because the single-particle density matrix has only one macroscopic eigenvalue [77]. We note that there is only one *physical* simple BEC ground state. In other words, all

bosons are condensed in the single mode $b_1^\dagger = \cos \frac{\varphi}{2} b_{\mathbf{0},\uparrow}^\dagger + i \sin \frac{\varphi}{2} b_{\boldsymbol{\pi},\uparrow}^\dagger$, where the continuous variable φ parametrizes the gauge orbit of physically equivalent simple BEC solutions. This simple BEC solution, for a particular gauge choice, can be selected by adding the infinitesimal ‘‘symmetry-breaking field’’ term

$$t \sum_{(ij),\sigma} [C_{ij}^\dagger(\varphi) + C_{ij}(\varphi)]$$

to the mean-field Hamiltonian with

$$C_{ij}^\dagger(\varphi) = \frac{1}{2} \mathbf{b}_i^\dagger(\boldsymbol{\sigma} \cdot \mathbf{n}(\varphi)) \mathbf{b}_j$$

in the global reference frame and $\mathbf{n}(\varphi) = (\cos \varphi, \sin \varphi, 0)$. We note that this operator transforms like a triplet under SU(2) rotations and breaks the U(1) symmetry of global rotations about the z -axis. In the twisted reference frame, the triplet bond operator $C_{ij}^\dagger(\varphi)$ becomes

$$C_{ij}^\dagger(\varphi) = -\frac{1}{2} \sum_{\sigma} e^{-i\sigma\eta_i\varphi} \sigma b_{i\sigma}^\dagger b_{j\sigma}.$$

For the gauge choice $\varphi = 0$, the simple BEC state $|G_3\rangle$ can be expressed as

$$|G_3\rangle = \frac{1}{u_{\mathbf{0}\uparrow}} e^{-\frac{v_{\mathbf{0}\uparrow}^*}{2u_{\mathbf{0}\uparrow}^*} \hat{b}_{\mathbf{0}\uparrow}^\dagger \hat{b}_{\mathbf{0}\uparrow}^\dagger} \prod_{(\mathbf{k},\sigma) \neq (\mathbf{0},\uparrow)} \frac{1}{u_{\mathbf{k}\sigma}} e^{-\frac{v_{\mathbf{k}\sigma}^*}{2u_{\mathbf{k}\sigma}^*} \hat{b}_{\mathbf{k}\sigma}^\dagger \hat{b}_{-\mathbf{k}\sigma}^\dagger} |\emptyset\rangle, \quad (69)$$

where, assuming $h, t \sim 1/\mathcal{N}_s$, the ratio $|v_{\mathbf{Q}\sigma}/u_{\mathbf{Q}\sigma}|$ satisfies $1 - |v_{\mathbf{Q}\sigma}/u_{\mathbf{Q}\sigma}| \propto 1/\mathcal{N}_s$ for $\mathbf{Q} = \mathbf{0}$ and $\sigma = \uparrow$, and $1 - |v_{\mathbf{Q}\sigma}/u_{\mathbf{Q}\sigma}| \propto 1/\mathcal{N}_s^{1/2}$ for the other three zero-energy modes. In other words, $|G_3\rangle$ describes a BEC with *macroscopic occupation of the single mode* $\mathbf{k} = \mathbf{0}$ and $\sigma = \uparrow$ [see Fig. 1(c)].

As we will see in the next subsection, while the ground states $|G_2\rangle$ and $|G_3\rangle$ correspond to ferromagnetic SP solutions in the twisted reference frame, they do not represent the same physical state because $\langle G_3 | \hat{O} | G_3 \rangle \neq \langle G_2 | \hat{O} | G_2 \rangle$ for some physical observables \hat{O} . Although these different condensates are degenerate at the SP level, fragmented BECs are known to be ‘‘fragile’’ against the inclusion of boson-boson interactions, which typically favor the simple BEC state [77,82]. This simple observation suggests that fluctuations of the HS fields should select the SP solution $|G_3\rangle$ corresponding to the simple BEC. Indeed, as we will see in Sec. VII, the expansion around the SP solution represented by the ground state $|G_2\rangle$ leads to a dynamical spin structure factor that is qualitatively incorrect for $\alpha \neq 0$ [the linear spin-wave theory (LSWT) result is not recovered in the large- S limit]. In contrast, the large- S limit of the dynamical spin structure factor that is obtained by including fluctuations around the simple BEC SP solution represented by the state $|G_3\rangle$ coincides with the LSWT result.

2. Physical character of candidate ground states

The invariance of $|G_1\rangle$ under global SU(2) spin rotations in the original reference frame implies that the local magnetization is zero for this SP solution. In contrast, the ground state $|G_2\rangle$ is U(1)-invariant under global (staggered) spin rotations about the z axis in the original (twisted) reference frame, which is compatible with a finite local magnetization $\mathbf{m} = m\hat{z}$ with $m = n_c/2$. The ground state $|G_3\rangle$ is invariant under a composition of the same U(1) spin rotation by an angle

φ about the z axis and the staggered gauge transformation $C(-\varphi)$ introduced in Eq. (59). In other words, $\mathcal{U}_z(\varphi)|G_3\rangle \sim C(\varphi)|G_3\rangle$ generates an orbit of gauge equivalent states. Although the local magnetization is also $\mathbf{m} = m\hat{z}$ with $m = n_c/2$, the states $|G_2\rangle$ and $|G_3\rangle$ are not connected by a gauge transformation. For instance, the two states have different expectation values of on-site spin correlation functions:

$$\begin{aligned} \langle G_2 | \hat{S}_i^\perp \cdot \hat{S}_i^\perp | G_2 \rangle &= S(S+1) - m^2, \\ \langle G_3 | \hat{S}_i^\perp \cdot \hat{S}_i^\perp | G_3 \rangle &= S(S+1) - m^2, \\ \langle G_2 | \hat{S}_i^z \hat{S}_i^z | G_2 \rangle &= \frac{1}{2}S(S+1) + \frac{1}{2}m^2, \\ \langle G_3 | \hat{S}_i^z \hat{S}_i^z | G_3 \rangle &= \frac{1}{2}S(S+1) + \frac{3}{2}m^2, \end{aligned} \quad (70)$$

where $\hat{S}_i^\perp = (\hat{S}_i^x, \hat{S}_i^y)$ are the transverse components of the spin operator relative to the magnetization axis. We note that these expectation values are independent of α . The resulting expectation value of $\hat{S}_i \cdot \hat{S}_i$ that determines the sum rule of the dynamical spin structure factor *at the SP level* is

$$\begin{aligned} \langle G_2 | \hat{S}_i \cdot \hat{S}_i | G_2 \rangle &= 3S(S+1)/2 - m^2/2, \\ \langle G_3 | \hat{S}_i \cdot \hat{S}_i | G_3 \rangle &= 3S(S+1)/2 + m^2/2. \end{aligned} \quad (71)$$

Both results are different from the one obtained for the SU(2)-invariant condensate: $\langle G_1 | \hat{S}_i \cdot \hat{S}_i | G_1 \rangle = 3S(S+1)/2$. Clearly, the three condensates violate the identity $\hat{S}_i \cdot \hat{S}_i = S(S+1)$ [Casimir operator of SU(2)] because the local constraint Eq. (2) is only imposed at the mean-field level. This shortcoming of the SP approximation leads to a well-known violation of the sum rule of the dynamical spin structure factor because its integral over momentum and frequency is equal to $\langle \hat{S}_i \cdot \hat{S}_i \rangle$ [2]. In other words, according to Eqs. (71), the frequency and momentum integral of the spectral weight is overestimated by approximately 50% [exactly 50% for the SU(2)-invariant condensate]. As we will see in Sec. VII, the sum rule is recovered to a much better approximation upon including fluctuations around the SP solution $|G_3\rangle$, and this result remains basically independent of α .

Hereafter, we will consider a simple BEC SP solution $|G_3\rangle$ for reasons that will become clear upon including $1/N$ corrections. For concreteness, we will adopt the gauge in which the bosons condense at the single-spinon $\mathbf{Q} = \mathbf{0}$ state, which is invariant under spatial inversion.

For later use, we introduce the “bare” or SP single-spinon Green’s function that is obtained with the simple condensate SP solution $|G_3\rangle$:

$$\mathcal{G}_{\text{SP}}(\mathbf{q}, i\omega_n) = \mathcal{G}_n(\mathbf{q}, i\omega_n) + \mathcal{G}_c(\mathbf{q}, i\omega_n). \quad (72)$$

The first term describes the noncondensed spinon at $(\mathbf{q}, \sigma) \neq (\mathbf{0}, 1)$, which is equal to the inverse of the dynamical matrix

$$\mathcal{G}_n(q) = [2\mathcal{M}(q)]^{-1} = \sum_{\sigma=\pm 1} \frac{g_{q\sigma}^-}{\varepsilon_{q\sigma} - i\omega_n} + \frac{g_{q\sigma}^+}{\varepsilon_{-q\sigma} + i\omega_n}, \quad (73)$$

where $g_{q\sigma}^- = X_{q\sigma} X_{q\sigma}^\dagger$ and $g_{q\sigma}^+ = \bar{X}_{q\sigma} \bar{X}_{q\sigma}^\dagger$. The second term arises from the condensed boson

$$\begin{aligned} \mathcal{G}_c(\mathbf{q}, i\omega_n) &= \mathcal{N}_s g_c^Q \delta_{\mathbf{q}, \mathbf{Q}} \left(\frac{1}{\varepsilon_c - i\omega_n} + \frac{1}{\varepsilon_c + i\omega_n} \right) \\ &\stackrel{\mathcal{N}_s \rightarrow \infty}{=} (2\pi)^3 g_c^Q \delta(\mathbf{q} - \mathbf{Q}) \delta(\omega_n), \end{aligned} \quad (74)$$

where $\mathbf{Q} = \mathbf{0}$, $g_c^Q = |c_Q\rangle \langle c_Q|$ with $|c_Q\rangle \equiv \lim_{\mathcal{N}_s \rightarrow \infty} X_{\mathbf{Q}, +1} / \sqrt{\mathcal{N}_s} = \sqrt{n_c} (1, 0, -1, 0)^T$. The second line of Eq. (74) corresponds to the thermodynamic limit in which the finite-size gap of the single-spinon eigenstate with $\mathbf{Q} = \mathbf{0}$ and $\sigma = +1$ goes to zero: $\varepsilon_c \rightarrow 0^+$.

D. Dynamical spin structure factor

1. General formulation

Our next goal is to compute the DSSF in the SP approximation. We will present the result for arbitrary values of N because in a later section we will consider higher-order corrections in powers of $1/N$. The first step is to introduce a Zeeman coupling to an external time- and space-dependent magnetic field, i.e., to add source terms to the action

$$NS_s = -\frac{1}{2} \int_0^\beta d\tau \sum_{j\mu} h_j^\mu(\tau) \psi_j^\dagger(\tau) u^\mu \psi_j(\tau), \quad (75)$$

where $\frac{1}{2} \psi_j^\dagger u^\mu \psi_j \equiv S_j^\mu$ represents the μ component of the spin at lattice site j [note that we are using a single index μ to denote the generators of Sp($N/2$)]. This source term modifies the dynamical matrix to $\mathcal{M}_h(k; p) = \mathcal{M}(k; p) - 1/(\sqrt{\mathcal{N}_s \beta}) h_{k-p}^\mu u^\mu$, whose first derivative with respect to the field h_{k-p}^μ gives rise to the external vertices

$$u^\mu(k, p) = -\left(\frac{1}{\sqrt{\mathcal{N}_s \beta}} \right)^{-1} \frac{\delta \mathcal{M}_h(k; p)}{\delta h_{k-p}^\mu}. \quad (76)$$

The dynamical magnetic susceptibility is then given by

$$\chi^{\mu\nu}(q) = \frac{\delta^2 \ln \mathcal{Z}_h}{\delta h_{-q}^\mu \delta h_q^\nu}, \quad (77)$$

where h_q^μ is the Fourier component of the external fields $h_i^\mu(\tau)$ and,

$$\mathcal{Z}_h = \int \mathcal{D}[\bar{W} W \lambda] \mathcal{D}[\bar{b} b] \exp(-N(S + S_s)).$$

According to the fluctuation-dissipation theorem [83], the DSSF is related to the imaginary part of the magnetic susceptibility. At zero temperature, we have

$$S^{\mu\nu}(\mathbf{q}, \omega) = \frac{1}{\pi} \Theta(\omega) \text{Im}[\chi^{\mu\nu}(\mathbf{q}, \omega)], \quad (78)$$

with $\Theta(\omega)$ being the Heaviside step function.

At the SP level, the dynamical magnetic susceptibility is obtained by taking the second functional derivative of $\ln(\mathcal{Z}_{h, \text{SP}})$ with respect to h :

$$\begin{aligned} \chi_{\text{SP}}^{\mu\nu}(q) &= \frac{1}{\mathcal{N}_s \beta} \sum_k \frac{1}{2} \text{Tr}[\mathcal{G}_n(k) u^\mu \mathcal{G}_n(k+q) u^\nu] \\ &+ \frac{1}{\mathcal{N}_s \beta} \sum_k \frac{1}{2} \text{Tr}[\mathcal{G}_c(k) u^\mu \mathcal{G}_n(k+q) u^\nu] \\ &+ \frac{1}{\mathcal{N}_s \beta} \sum_k \frac{1}{2} \text{Tr}[\mathcal{G}_n(k) u^\mu \mathcal{G}_c(k+q) u^\nu] \\ &+ \frac{1}{\mathcal{N}_s \beta} \sum_k \frac{1}{2} \text{Tr}[\mathcal{G}_c(k) u^\mu \mathcal{G}_c(k+q) u^\nu], \end{aligned} \quad (79)$$

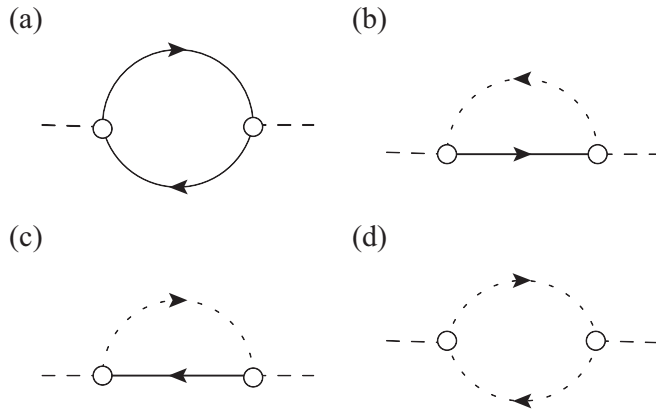


FIG. 2. Diagrammatic representation of the four contributions to the dynamical spin susceptibility $\chi_{\text{SP}}^{\mu\nu}(\mathbf{q})$ at the SP level corresponding to the four terms of Eq. (79). The full (dashed) line represents the propagator of the noncondensed (condensed) spinons. The open circles represent the external vertices of the theory introduced in Eq. (76).

which can be decomposed into four contributions represented by the four diagrams (a)–(d) in Fig. 2. The full lines represent the normal contribution to the Green's functions from noncondensed spinon, while the dashed lines represent the contribution from the spinon condensate. Consequently, the one-loop diagram (a) generates spectral weight from the two-spinon continuum, while the tree-level diagrams (b) and (c) generate δ -peaks in the DSSF (poles of the magnetic susceptibility) at the single-spinon energy $\omega = \varepsilon_{q_n}$.

The Green's function \mathcal{G}_c is a rank-1 matrix for the simple BEC ground state given by Eq. (74) with $|c_{\mathbf{Q}}\rangle$ being a $2N$ -vector now. The noncondensed Green's function is given by Eq. (73), where $g_{q_n}^+ = |n, \mathbf{Q} + \mathbf{q}\rangle \langle n, \mathbf{Q} + \mathbf{q}|$, and $g_{q_n}^- = P(g_{-q_n}^+)^* P$. The tree-level contribution to $\chi_{\text{SP}}^{\mu\nu}$, i.e., the second and third terms of Eq. (79), can be written in a simple form by using the following identity:

$$\text{Tr}[F] = \sum_{n=1}^{2N} \gamma_{nm}^0 \langle n | \gamma^0 F | n \rangle, \quad (80)$$

where the state vectors are normalized according to $\gamma_{nm}^0 \equiv \langle n | \gamma^0 | m \rangle$, and F is an arbitrary $2N \times 2N$ complex matrix. Using this relation, we obtain

$$\chi_{\text{SP},b}^{\mu\nu}(\mathbf{q}, i\omega_n) = \frac{1}{2} \langle c_{\mathbf{Q}} | u^\mu \mathcal{G}_n(\mathbf{Q} + \mathbf{q}, i\omega_n) u^\nu | c_{\mathbf{Q}} \rangle, \quad (81)$$

$$\chi_{\text{SP},c}^{\mu\nu}(\mathbf{q}, i\omega_n) = \frac{1}{2} \langle c_{\mathbf{Q}} | u^\nu \mathcal{G}_n(\mathbf{Q} - \mathbf{q}, -i\omega_n) u^\mu | c_{\mathbf{Q}} \rangle, \quad (82)$$

where $\chi_{\text{SP},b}^{\mu\nu}(\mathbf{q}, i\omega_n)$ is the contribution from diagram (b) of Fig. 2 that has poles at $i\omega_n = \varepsilon_{\mathbf{Q}+q_n}$, while $\chi_{\text{SP},c}^{\mu\nu}(\mathbf{q}, i\omega_n)$ is the contribution from diagram (c) of Fig. 2 that has poles at $i\omega_n = \varepsilon_{\mathbf{Q}-q_n}$, $n = 1, \dots, N$.

Particle-hole symmetry dictates that $|c_{\mathbf{Q}}\rangle$, the spinon Green's function, and the external/internal vertices must satisfy

$$P|c_{\mathbf{Q}}\rangle^* = |c_{\mathbf{Q}}\rangle, \quad P\mathcal{G}_n(-\mathbf{q}, -\omega)^T P = \mathcal{G}_n(\mathbf{q}, \omega), \quad (83)$$

$$P(u^\mu)^T P = u^\mu, \quad P[v_\alpha(\mathbf{k}, \mathbf{q})]^T P = v_\alpha(-\mathbf{q}, -\mathbf{k}). \quad (84)$$

From these relations and the property $\mathbf{Q} \equiv -\mathbf{Q}$, we can demonstrate that $\chi_{\text{SP},b}^{\mu\nu} = \chi_{\text{SP},c}^{\mu\nu}$. The residue associated with the SP pole $\varepsilon_{\mathbf{Q}+q_n} = \varepsilon_{q_n}$ is

$$Z_{\text{SP}}^{\mu\nu}(n, \mathbf{q}) = \lim_{\omega \rightarrow \varepsilon_{q_n}} (\varepsilon_{q_n} - \omega) \chi_{\text{SP}}^{\mu\nu}(\mathbf{q}, \omega) = g_\mu^{\mathbf{Q}}(n, \mathbf{q}) \overline{g}_\nu^{\mathbf{Q}}(n, \mathbf{q}), \quad (85)$$

where

$$g_\mu^{\mathbf{Q}}(n, \mathbf{q}) = \langle c_{\mathbf{Q}} | u^\mu | n, \mathbf{Q} + \mathbf{q} \rangle, \quad (86)$$

$$\overline{g}_\nu^{\mathbf{Q}}(n, \mathbf{q}) = \langle n, \mathbf{Q} + \mathbf{q} | u^\nu | c_{\mathbf{Q}} \rangle. \quad (87)$$

Diagram (d) of Fig. 2 contributes only to the static and uniform (in the twisted reference frame) component of the dynamical spin structure factor. Its spectral weight is proportional to the number of lattice sites, implying that it diverges in the thermodynamic limit. On a finite lattice with a symmetry-breaking field $\propto \mathcal{N}_s^{-1}$, it is given by

$$\chi_{\text{SP},d}^{\mu\nu}(\mathbf{q}, i\omega_n) = \frac{1}{2} \mathcal{N}_s \delta_{\mathbf{q},0} \langle c_{\mathbf{Q}} | u^\mu | c_{\mathbf{Q}} \rangle \langle c_{\mathbf{Q}} | u^\nu | c_{\mathbf{Q}} \rangle \times \left(\frac{1}{2\varepsilon_c - i\omega_n} + \frac{1}{2\varepsilon_c + i\omega_n} \right), \quad (88)$$

where ε_c is of order $1/\mathcal{N}_s$.

2. Square lattice Heisenberg model

As an example, we apply the above results to the square lattice SU(2)-invariant antiferromagnetic Heisenberg model. The external vertices are independent of frequency and momentum:

$$u^x = \frac{1}{2} \begin{pmatrix} \sigma_x & 0 \\ 0 & \sigma_x^T \end{pmatrix}, \quad (89)$$

$$u^y = \frac{1}{2} \begin{pmatrix} \sigma_y & 0 \\ 0 & \sigma_y^T \end{pmatrix}, \quad (90)$$

$$u^z = \frac{1}{2} \begin{pmatrix} \sigma_z & 0 \\ 0 & \sigma_z^T \end{pmatrix}. \quad (91)$$

In particular, we consider the semiclassical limit of the ground state $|G_3\rangle$ by taking $S \rightarrow \infty$, for which the dynamical magnetic susceptibility is exactly described by the LSWT. For $S \rightarrow \infty$, the SP approximation of the Schwinger boson theory gives $n_c = 2S$, $A_x = 2S$, $B_x = 0$, and $\lambda = 4JS(1 - \alpha)$, which makes $\mathcal{G}_n \sim S^{-1}$ and $\mathcal{G}_c \sim S^0$. Consequently, the DSSF has zero spectral weight in the two-spinon continuum and finite spectral weight at the single-spinon dispersion (poles of the SP Green's function). In other words, in the large- S limit, the contribution from the diagram shown in Fig. 2(a) is negligible in comparison to the contributions from the diagrams shown Figs. 2(b)–2(d). After performing the analytic continuation $i\omega_n \rightarrow \omega + i0^+$ to real frequency and converting the result back to the original reference frame, we obtain

$$\chi_{\text{SP}}^{\text{xx}}(\mathbf{q}, \omega) = \chi_{\text{SP}}^{\text{yy}}(\mathbf{q}, \omega) = S \sqrt{\frac{1 - \gamma_q^+}{1 + \gamma_q^+}} \frac{1}{2} \left(\frac{1}{\varepsilon_q - \omega - i0^+} + \frac{1}{\varepsilon_q + \omega + i0^+} \right), \quad (92)$$

$$\chi_{\text{SP}}^{zz}(\mathbf{q}, \omega) = \chi_{\text{SP}}^{xx}(\mathbf{q}, \omega) + \frac{\mathcal{N}_s n_c^2}{2} \delta_{\mathbf{q}, \pi} \left(\frac{1}{2\varepsilon_c - \omega - i0^+} + \frac{1}{2\varepsilon_c + \omega + i0^+} \right), \quad (93)$$

where $\varepsilon_q = (1 - \alpha)\omega_q$, and ω_q is the single-magnon dispersion that is obtained with LSWT for the square lattice AFM Heisenberg model. We note that the diagrams shown in Figs. 2(b) and 2(c) produce an SU(2)-invariant contribution to the magnetic susceptibility that is the same for the three different ground states, while the diagram shown in Fig. 2(d) breaks the SU(2) invariance explicitly and leads to the finite difference $\chi_{\text{SP}}^{zz}(\mathbf{q}, \omega) - \chi_{\text{SP}}^{xx/yy}(\mathbf{q}, \omega)$ for the ground states $|G_2\rangle$ and $|G_3\rangle$. We also note that different choices of α , i.e., different decoupling schemes of the original Hamiltonian, lead to different SP approximations: $\chi_{\text{SP}}^{xx}(\mathbf{q}, \omega)$ and $\chi_{\text{SP}}^{yy}(\mathbf{q}, \omega)$ coincide with the LSWT result only for $\alpha = 0$ [7].

There is also an important qualitative difference between the SP approximation of the SB theory and LSWT. The inelastic contribution to the SP susceptibility, arising from the bubble diagrams shown in Figs. 2(b) and 2(c), is SU(2)-invariant. This property leads to the result given in Eqs. (92) and (93), implying that the dynamical spin structure factor satisfies $S^{xx}(\mathbf{q}, \omega \neq 0) = S^{yy}(\mathbf{q}, \omega \neq 0) = S^{zz}(\mathbf{q}, \omega \neq 0)$. This *qualitatively incorrect* result must be contrasted with the LSWT, where only the transverse spin susceptibility has poles corresponding to magnons, while the longitudinal susceptibility only includes a two-magnon continuum with relative small spectral weight. This simple observation invalidates the association of the poles of the SP susceptibility with magnon modes. As we will show in Sec. VII, the correct LSWT result can be recovered by including corrections due to fluctuations around the SP solution [38].

V. BEYOND THE SADDLE-POINT APPROXIMATION

Fluctuations of the auxiliary fields (W, \bar{W}) and the Lagrangian multiplier (λ) around the SP configuration are described by the fluctuation fields

$$\phi_\alpha(q) = [W_\delta^\mu(q) - W_\delta^\mu(q)|_{\text{SP}}, \bar{W}_\delta^\mu(-q) - \bar{W}_\delta^\mu(-q)|_{\text{SP}}, \lambda(q) - \lambda(q)|_{\text{SP}}], \quad (94)$$

where α represents the field indices ($W_\delta^\mu, \bar{W}_\delta^\mu$ or λ).

The large- N expansion is then obtained by expanding the effective action Eq. (27) around the SP in powers of the fields $\phi_\alpha(q)$:

$$S_{\text{eff}} = S_{\text{eff}}^{\text{SP}} + \frac{1}{2} \sum_{q, \alpha_1, \alpha_2} S_{\alpha_1, \alpha_2}^{(2)}(q) \phi_{\alpha_1}(-q) \phi_{\alpha_2}(q) + S_{\text{int}}, \quad (95)$$

$$\begin{aligned} \Pi_{\alpha_1 \alpha_2}(\mathbf{q}, i\omega_n) &= \frac{1}{2c\mathcal{N}_s\beta} \sum_k \frac{1}{N} \text{Tr}[\mathcal{G}_n(k) v_{\alpha_1}(\mathbf{k}, \mathbf{k} + \mathbf{q}) \mathcal{G}_n(k + q) v_{\alpha_2}(\mathbf{k} + \mathbf{q}, \mathbf{k})] \\ &+ \frac{1}{2c\mathcal{N}_s\beta} \sum_k \frac{1}{N} \text{Tr}[\mathcal{G}_c(k) v_{\alpha_1}(\mathbf{k}, \mathbf{k} + \mathbf{q}) \mathcal{G}_n(k + q) v_{\alpha_2}(\mathbf{k} + \mathbf{q}, \mathbf{k})] \\ &+ \frac{1}{2c\mathcal{N}_s\beta} \sum_k \frac{1}{N} \text{Tr}[\mathcal{G}_n(k) v_{\alpha_1}(\mathbf{k}, \mathbf{k} + \mathbf{q}) \mathcal{G}_c(k + q) v_{\alpha_2}(\mathbf{k} + \mathbf{q}, \mathbf{k})] \\ &+ \frac{1}{2c\mathcal{N}_s\beta} \sum_k \frac{1}{N} \text{Tr}[\mathcal{G}_c(k) v_{\alpha_1}(\mathbf{k}, \mathbf{k} + \mathbf{q}) \mathcal{G}_c(k + q) v_{\alpha_2}(\mathbf{k} + \mathbf{q}, \mathbf{k})]. \end{aligned} \quad (102)$$

with

$$S_{\text{int}} = \sum_{n \geq 3} \frac{1}{n!} \sum_{\substack{\alpha_1 \dots \alpha_n \\ q_{1n}}} S_{\alpha_1 \dots \alpha_n}^{[n]}(q_1, \dots, q_n) \phi_{\alpha_1}(q_1) \dots \phi_{\alpha_n}(q_n),$$

where the first term is the SP contribution, the second (quadratic) term corresponds to the usual random phase approximation (RPA), and the last term describes the interaction between the fluctuation fields [2,38].

The coefficients of the quadratic form can be expressed as

$$S^{(2)}(q) = \Pi_0 - \Pi(q), \quad (96)$$

where

$$\begin{aligned} (\Pi_0)_{\alpha_1 \alpha_2} &= \frac{1 - \alpha}{4J_\delta} (\delta_{\alpha_1, \bar{W}_\delta^A} \delta_{\alpha_2, W_\delta^A} + \delta_{\alpha_1, W_\delta^A} \delta_{\alpha_2, \bar{W}_\delta^A}) \\ &+ \frac{\alpha}{4J_\delta} (\delta_{\alpha_1, \bar{W}_\delta^B} \delta_{\alpha_2, W_\delta^B} + \delta_{\alpha_1, W_\delta^B} \delta_{\alpha_2, \bar{W}_\delta^B}), \end{aligned} \quad (97)$$

and the polarization operator is

$$\begin{aligned} \Pi_{\alpha_1 \alpha_2}(q) &= \frac{1}{2c\mathcal{N}_s\beta} \sum_k \frac{1}{N} \text{Tr}[\mathcal{G}_{\text{SP}}(k) v_{\alpha_1}(\mathbf{k}, \mathbf{k} + \mathbf{q}) \mathcal{G}_{\text{SP}}(k + q) \\ &\times v_{\alpha_2}(\mathbf{k} + \mathbf{q}, \mathbf{k})]. \end{aligned} \quad (98)$$

The RPA propagator of the fluctuation fields is given by

$$\begin{aligned} \frac{1}{N} [D_{\alpha_1 \alpha_2}](q) &= \frac{1}{\mathcal{Z}^{(2)}} \int \mathcal{D}[\phi] \phi_{\alpha_1}(q) \phi_{\alpha_2}(-q) \\ &\times e^{-\frac{N}{2} \sum_{q, \alpha_1, \alpha_2} S_{\alpha_1, \alpha_2}^{(2)}(q) \phi_{\alpha_1}(-q) \phi_{\alpha_2}(q)} \\ &= [(NS^{(2)})^{-1}]_{\alpha_1 \alpha_2}, \end{aligned} \quad (99)$$

where

$$\mathcal{Z}^{(2)} = \int \mathcal{D}[\phi] e^{-\frac{N}{2} \sum_{q, \alpha_1, \alpha_2} S_{\alpha_1, \alpha_2}^{(2)}(q) \phi_{\alpha_1}(-q) \phi_{\alpha_2}(q)}. \quad (100)$$

The coefficients of the higher-order corrections ($n \geq 3$) are

$$S_{\alpha_1 \dots \alpha_n}^{[n]}(q_1, \dots, q_n) = \frac{(-1)^{n+1}}{n(c\mathcal{N}_s\beta)^{\frac{n}{2}}} \frac{1}{N} \sum_P \text{Tr}[\mathcal{G}_{\text{SP}} v_{P_1} \dots \mathcal{G}_{\text{SP}} v_{P_n}], \quad (101)$$

where \sum_P runs over all permutations of the particle index (α_i, q_i), $1 \leq i \leq n$, which symmetrizes the vertex function relative to the exchange of any pair of particles.

A. RPA propagator

Because of the spinon condensation, the polarization operator in Eq. (98) also includes four contributions,

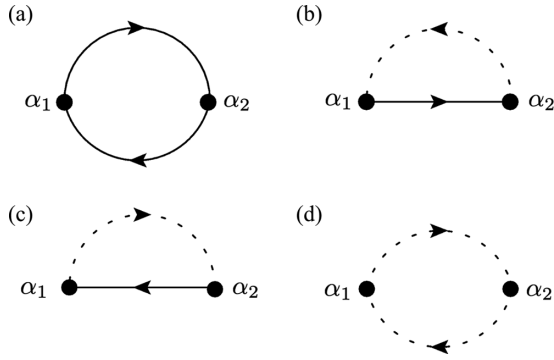


FIG. 3. Diagrammatic representation of the four contributions to the polarization operator $\Pi(\mathbf{q}, i\omega_n)$ corresponding to the four terms of Eq. (102). The full circles represent the internal vertices of the theory introduced in Eq. (25).

The first term corresponds to the one-loop Feynman diagram shown in Fig. 3(a). The rest of the terms include at least one contribution from the condensed spinons, implying that they only exist in the magnetically ordered phase. In particular, the second and the third terms, represented by the tree-level diagrams shown in Figs. 3(b) and 3(c), are equal because of the same symmetry arguments that lead to the equivalence between the diagrams shown in Figs. 2(b) and 2(c):

$$\begin{aligned} \Pi_{\alpha_1\alpha_2}^{(b)}(\mathbf{q}, i\omega_n) &= \Pi_{\alpha_1\alpha_2}^{(c)}(\mathbf{q}, i\omega_n) \\ &= \frac{1}{2N} \langle c_{\mathbf{Q}} | v_{\alpha_1}(\mathbf{Q}, \mathbf{Q} + \mathbf{q}) \mathcal{G}_n(\mathbf{Q} + \mathbf{q}, i\omega_n) \\ &\quad \times v_{\alpha_2}(\mathbf{Q} + \mathbf{q}, \mathbf{Q}) | c_{\mathbf{Q}} \rangle. \end{aligned} \quad (103)$$

The last term of Eq. (102), corresponding to the diagram shown in Fig. 3(d), has only zero-frequency and momentum ($\omega = 0, \mathbf{q} = \mathbf{0}$) components:

$$\begin{aligned} \Pi_{\alpha_1\alpha_2}^{(d)}(\mathbf{q}, i\omega_n) &= (2\pi)^3 \delta(\omega_n) \delta(\mathbf{q}) \\ &\quad \times \frac{1}{2N} \langle c_{\mathbf{Q}} | v_{\alpha_1}(\mathbf{Q}, \mathbf{Q}) | c_{\mathbf{Q}} \rangle \langle c_{\mathbf{Q}} | v_{\alpha_2}(\mathbf{Q}, \mathbf{Q}) | c_{\mathbf{Q}} \rangle. \end{aligned} \quad (104)$$

VI. CANCELLATION OF SINGLE-SPINON POLES

The primary purpose of this section is to demonstrate that the spectral weight of $\chi_{\text{SP}}^{\mu\nu}$ at the single-spinon poles, $\omega = \varepsilon_{\mathbf{q}n}$, is exactly canceled out by a counterdiagram that is *nominally* of order $1/N$. By “nominally” here we mean the well-defined order $1/N^{P-L}$ (L is the number of internal loops and P is the number of RPA propagators) that the diagram would have *in the absence of a condensate* [2]. Naively, this cancellation is unexpected because a $1/N$ contribution cannot cancel a contribution of order $1/N^0$ for arbitrary values of N . The crucial observation is that the classification of the Feynman diagrams in powers of $1/N$ [2] does not take into consideration singular contributions that are generated by the finite condensate fraction. In other words, diagrams that are nominally of order $1/N$ include a singular contribution of order $O(1/N^0)$ whenever the condensate fraction n_c is finite. This contribution corresponds

to isolated poles with residues of $O(1/N^0)$ that exactly cancel out the poles of the SP solution.

In previous works on the triangular Heisenberg antiferromagnet, we reported this cancellation for one specific diagram of order $1/N$ [38]. Here we will reveal the origin of the cancellation and generalize the result to other diagrams. From a physical point of view, this exact cancellation simply means that spinons are not quasiparticles of the magnetically ordered state. The true quasiparticles are magnons (two-spinon bound states) arising from poles of the RPA propagator [37,38].

A. $1/N$ corrections

The $1/N$ correction we considered in previous works [37,38] is given by

$$\chi_{\text{FL}}^{\mu\nu}(\mathbf{q}) = \sum_{\alpha_1\alpha_2} \Lambda^{\mu\alpha_1}(\mathbf{q}) \frac{1}{N} D_{\alpha_1\alpha_2}(\mathbf{q}) \Lambda^{\nu\alpha_2}(-\mathbf{q}), \quad (105)$$

where

$$\Lambda^{\mu\alpha_1}(\mathbf{q}) = \frac{1}{2\mathcal{N}_s\beta} \sum_{\mathbf{k}} \text{Tr}[\mathcal{G}_{\text{SP}}(\mathbf{k}) u^\mu \mathcal{G}_{\text{SP}}(\mathbf{k} + \mathbf{q}) v_{\alpha_1}(\mathbf{k} + \mathbf{q}, \mathbf{k})]. \quad (106)$$

This contribution is represented by the diagrams shown in Fig. 4. We will first demonstrate that the poles of $\chi_{\text{SP}}^{\mu\nu}$ are canceled by these diagrams, which represent different contributions to a diagram of nominal order $1/N$ in the large- N expansion of the magnetic susceptibility [37,38]. We have split this diagram into a sum of different subdiagrams because the spinon and the RPA propagators include condensed and noncondensed contributions represented with different types of lines. Similarly to Fig. 2, the full (dashed) line represents the propagator of the noncondensed (condensed) spinons, while the black wavy line represents the RPA propagator.

Since the diagram includes two loops, and each loop includes two spinon propagators, there are four tree-level diagrams shown in Figs. 4(a2)–4(a5) that have poles of the noncondensed spinon line and of the RPA propagator. They are called “tree-level” diagrams simply because the condensed spinon line carries fixed momentum \mathbf{Q} and zero Matsubara frequency $i\omega_n = 0$, which is equivalent to a classical external potential. The diagram shown in Fig. 4(a1) only includes spectral weight from the two-spinon continuum, while the diagram shown in Fig. 4(a6) corresponds to an elastic ($\omega = 0$) contribution. Our main focus is on the pole singularities that arise from the noncondensed single-spinon propagators in the diagrams shown in Figs. 4(a2)–4(a5). The particle-hole symmetry that leads to Eqs. (83) and (84) implies that these four diagrams give identical contributions $\chi_{\text{FL};(a2-a5)}^{\mu\nu}(\mathbf{q}, \omega)$ to the dynamical spin susceptibility with

$$\begin{aligned} \Lambda_{(a2-a5)}^{\mu\alpha_1}(\mathbf{q}, \omega) &= \frac{1}{2\mathcal{N}_s\beta} \sum_{\mathbf{k}} \text{Tr}[\mathcal{G}_c(\mathbf{k}) u^\mu \mathcal{G}_n(\mathbf{k} + \mathbf{q}) v_{\alpha_1}(\mathbf{k} + \mathbf{q}, \mathbf{k})] \\ &\quad + \frac{1}{2\mathcal{N}_s\beta} \sum_{\mathbf{k}} \text{Tr}[\mathcal{G}_n(\mathbf{k}) u^\mu \mathcal{G}_c(\mathbf{k} + \mathbf{q}) v_{\alpha_1}(\mathbf{k} + \mathbf{q}, \mathbf{k})]. \end{aligned}$$

Consequently,

$$\begin{aligned} \chi_{\text{FL};(a2-a5)}^{\mu\nu}(\mathbf{q}, \omega) = & \frac{1}{4N} [\langle c_{\mathbf{Q}} | u^\mu \mathcal{G}_n(\mathbf{q} + \mathbf{Q}, \omega) v_{\alpha_1}(\mathbf{q} + \mathbf{Q}, \mathbf{Q}) | c_{\mathbf{Q}} \rangle + \langle c_{\mathbf{Q}} | v_{\alpha_1}(\mathbf{Q}, -\mathbf{q} + \mathbf{Q}) \mathcal{G}_n(-\mathbf{q} + \mathbf{Q}, -\omega) u^\mu | c_{\mathbf{Q}} \rangle] \\ & \times D_{\alpha_1\alpha_2}(\mathbf{q}, \omega) [\langle c_{\mathbf{Q}} | v_{\alpha_2}(\mathbf{Q}, \mathbf{q} + \mathbf{Q}) \mathcal{G}_n(\mathbf{q} + \mathbf{Q}, \omega) u^\nu | c_{\mathbf{Q}} \rangle + \langle c_{\mathbf{Q}} | u^\nu \mathcal{G}_n(-\mathbf{q} + \mathbf{Q}, -\omega) v_{\alpha_2}(-\mathbf{q} + \mathbf{Q}, \mathbf{Q}) | c_{\mathbf{Q}} \rangle]. \end{aligned} \quad (107)$$

It is clear that, like $\chi_{\text{SP}}^{\mu\nu}(\mathbf{q}, \omega)$ (see Fig. 2), $\chi_{\text{FL};(a2-a5)}^{\mu\nu}(\mathbf{q}, \omega)$ has poles at the single-spinon energies ε_{q_n} arising from loops with one dashed and one full line. For the four diagrams, the residue of this pole reads

$$Z_{\text{FL}}^{\mu\nu}(n, \mathbf{q}) = \lim_{\omega \rightarrow \varepsilon_{q_n}} (\varepsilon_{q_n} - \omega) \chi_{\text{FL}}^{\mu\nu}(\mathbf{q}, \omega) = \frac{1}{-i\eta N} g_\mu^{\mathbf{Q}}(n, \mathbf{q}) \overline{g_\nu^{\mathbf{Q}}}(n, \mathbf{q}) \langle n, \mathbf{Q} + \mathbf{q} | \Sigma(\mathbf{Q} + \mathbf{q}, \varepsilon_{q_n}) | n, \mathbf{Q} + \mathbf{q} \rangle, \quad (108)$$

where η is an infinitesimal positive number that arises from the pole of the single-spinon Green's function, $\lim_{\omega \rightarrow \varepsilon_{q_n}} 1/(\varepsilon_{q_n} - \omega - i\eta)$, and the matrix element is given by

$$\langle n, \mathbf{Q} + \mathbf{q} | \Sigma(\mathbf{Q} + \mathbf{q}, \varepsilon_{q_n}) | n, \mathbf{Q} + \mathbf{q} \rangle = \sum_{\alpha_1\alpha_2} D_{\alpha_1\alpha_2}(\mathbf{q}, \varepsilon_{q_n}) \bar{f}_{\alpha_1}^{\mathbf{Q}}(n, \mathbf{q}) f_{\alpha_2}^{\mathbf{Q}}(n, \mathbf{q}) = \bar{\mathbf{f}}^{\mathbf{Q}}(n, \mathbf{q}) D(\mathbf{q}, \varepsilon_{q_n}) \mathbf{f}^{\mathbf{Q}}(n, \mathbf{q}), \quad (109)$$

where we have introduced the row and column vectors:

$$\mathbf{f}^{\mathbf{Q}}(n, \mathbf{q}) = [\langle c_{\mathbf{Q}} | v_1(\mathbf{Q}, \mathbf{Q} + \mathbf{q}) | n, \mathbf{Q} + \mathbf{q} \rangle, \dots, \langle c_{\mathbf{Q}} | v_{N_\phi}(\mathbf{Q}, \mathbf{Q} + \mathbf{q}) | n, \mathbf{Q} + \mathbf{q} \rangle], \quad \bar{\mathbf{f}}^{\mathbf{Q}}(n, \mathbf{q}) = \begin{bmatrix} \langle n, \mathbf{Q} + \mathbf{q} | v_1(\mathbf{Q} + \mathbf{q}, \mathbf{Q}) | c_{\mathbf{Q}} \rangle \\ \vdots \\ \langle n, \mathbf{Q} + \mathbf{q} | v_{N_\phi}(\mathbf{Q} + \mathbf{q}, \mathbf{Q}) | c_{\mathbf{Q}} \rangle \end{bmatrix}, \quad (110)$$

and N_ϕ is the number of flavors of the fluctuation fields ϕ_α . We note that $\mathbf{f}^{\mathbf{Q}}(n, \mathbf{q})$ and $\bar{\mathbf{f}}^{\mathbf{Q}}(n, \mathbf{q})$ are both proportional to the factor $\sqrt{n_c}$ carried by the ket $|c_{\mathbf{Q}}\rangle$.

According to Eq. (85), the condition for the cancellation of the pole of $\chi_{\text{SP}}^{\mu\nu}(\mathbf{q}, \omega)$ at ε_{q_n} is that the matrix element $\langle n, \mathbf{Q} + \mathbf{q} | \Sigma(\mathbf{Q} + \mathbf{q}, \varepsilon_{q_n}) | n, \mathbf{Q} + \mathbf{q} \rangle$ must be equal to $i\eta N$. In other words, as we will demonstrate below, ε_{q_n} must be a *zero* of the propagator $D(\mathbf{q}, \omega)$.

1. Anomalous large- N scaling of the RPA propagator

The RPA propagator is given by the inverse of the fluctuation matrix:

$$D(\mathbf{q}, \omega) = [\Pi_0 - \Pi(\mathbf{q}, \omega)]^{-1}. \quad (111)$$

The tree-level diagrams of the polarization operator $\Pi(\mathbf{q}, \omega)$ (see Fig. 3) have poles at $\omega = \varepsilon_{q_n}$, namely

$$\Pi_{\alpha_1\alpha_2}^{(b)}(\mathbf{q}, \varepsilon_{q_n}) = \Pi_{\alpha_1\alpha_2}^{(c)}(\mathbf{q}, \varepsilon_{q_n}) = \frac{1}{2N} \frac{1}{(-i\eta)} f_{\alpha_1}^{\mathbf{Q}}(n, \mathbf{q}) \bar{f}_{\alpha_2}^{\mathbf{Q}}(n, \mathbf{q}). \quad (112)$$

It is important to note that only the spinon from the n -band with momentum $\mathbf{Q} + \mathbf{q}$ contributes to the polarization operator, implying that $\Pi(\mathbf{q}, \varepsilon_{q_n}) \sim O(1/N)$.

Since the tree-level diagrams diverge at $\omega = \varepsilon_{q_n}$, we can neglect the regular contribution from the loop diagram shown in Fig. 3(a), and the polarization operator is dominated by a

rank-1 matrix,

$$\Pi_{\alpha_1\alpha_2}(\mathbf{q}, \varepsilon_{q_n}) = \frac{f_{\alpha_1}^{\mathbf{Q}}(n, \mathbf{q}) \bar{f}_{\alpha_2}^{\mathbf{Q}}(n, \mathbf{q})}{-i\eta N}. \quad (113)$$

To compute the RPA propagator, it is convenient to introduce a new pair of orthogonal bases $\{\boldsymbol{\mu}_\alpha\}$ and $\{\mathbf{v}_\alpha^\dagger\}$ such that the first vector of each basis is a unit vector parallel to $\mathbf{f}^{\mathbf{Q}}(n, \mathbf{q})$ and $\bar{\mathbf{f}}^{\mathbf{Q}}(n, \mathbf{q})$, respectively:

$$\boldsymbol{\mu}_1 = \frac{\mathbf{f}^{\mathbf{Q}}(n, \mathbf{q})}{\|\mathbf{f}^{\mathbf{Q}}(n, \mathbf{q})\|}, \quad \mathbf{v}_1^\dagger = \frac{\bar{\mathbf{f}}^{\mathbf{Q}}(n, \mathbf{q})}{\|\bar{\mathbf{f}}^{\mathbf{Q}}(n, \mathbf{q})\|}, \quad (114)$$

where $\|\mathbf{f}\|$ is the norm of the vector \mathbf{f} . The basis $\{\boldsymbol{\mu}_\alpha\}$ spans the left space of the fluctuation matrix $\Pi_0 - \Pi$, while $\{\mathbf{v}_\alpha^\dagger\}$ spans the right space. In the new basis, the fluctuation matrix

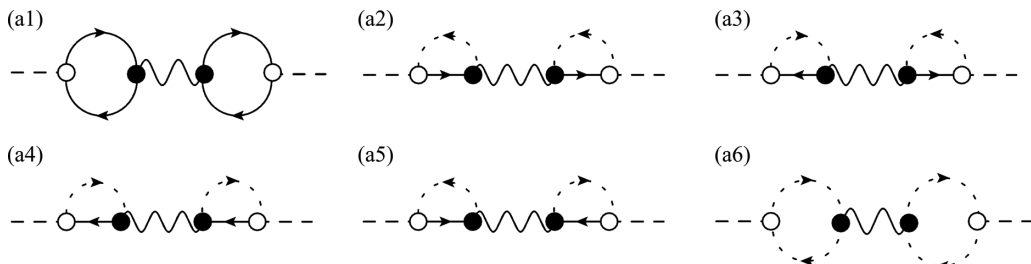


FIG. 4. $1/N$ diagrams of dynamical spin susceptibility. The wavy line refers to the RPA propagator $\frac{1}{N}D(\mathbf{q}, \omega)$.

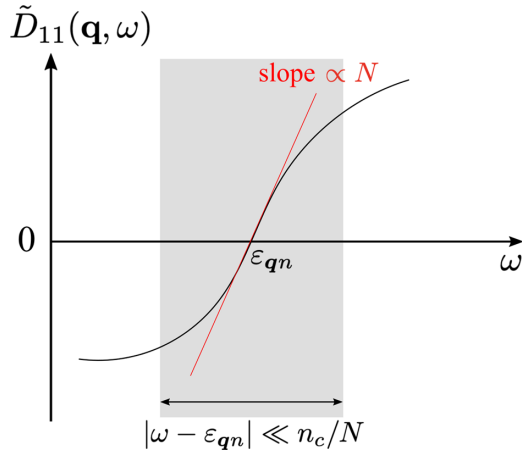


FIG. 5. Vicinity of the zero of $\tilde{D}_{11}(\mathbf{q}, \omega)$ (gray area) where the RPA propagator displays anomalous large- N scaling, namely $d\tilde{D}_{11}/d\omega|_{\omega=\epsilon_{qn}} \propto N$, as indicated by the red line.

is given by

$$\begin{aligned} \tilde{D}^{-1}(\mathbf{q}, \epsilon_{qn}) &= U^\dagger D^{-1}(\mathbf{q}, \epsilon_{qn}) V \\ &= \frac{\|\mathbf{f}^Q(n, \mathbf{q})\| \|\tilde{\mathbf{f}}^Q(n, \mathbf{q})\|}{i\eta N} I^{(1,1)} + O(\eta^0), \end{aligned} \quad (115)$$

where $I^{(1,1)}$ is the single-entry $N_\phi \times N_\phi$ matrix $I_{\alpha_1, \alpha_2}^{(1,1)} = \delta_{\alpha_1, 1} \delta_{\alpha_2, 1}$, and the column j of the unitary matrix U (V) is equal to the vector \mathbf{u}_j (\mathbf{v}_j):

$$U = [\boldsymbol{\mu}_1, \dots, \boldsymbol{\mu}_{N_\phi}], \quad V = [\mathbf{v}_1, \dots, \mathbf{v}_{N_\phi}]. \quad (116)$$

The (1,1) component $[\tilde{D}^{-1}(\mathbf{q}, \epsilon_{qn})]_{11}$ scales as n_c/N instead of the usual scaling $\sim N^0$ for a magnetically disordered state ($n_c = 0$). Since $n_c/(\eta N) \gg 1$ for an ordered magnet with $n_c \neq 0$, the inverse of Eq. (115) leads to

$$\begin{aligned} \tilde{D}_{11}(\mathbf{q}, \epsilon_{qn}) &\equiv \mathbf{v}_1^\dagger D(\mathbf{q}, \epsilon_{qn}) \boldsymbol{\mu}_1 \\ &= \frac{i\eta N}{\|\mathbf{f}^Q(n, \mathbf{q})\| \|\tilde{\mathbf{f}}^Q(n, \mathbf{q})\|} + O\left(\frac{\eta^2 N^2}{n_c^2}\right), \end{aligned} \quad (117)$$

implying that $\tilde{D}_{11}(\mathbf{q}, \epsilon_{qn}) \propto N$ instead of the N^0 scaling that is obtained in the absence of spinon condensation. Since $i\eta = \omega - \epsilon_{qn}$ is an infinitesimal number, $\omega = \epsilon_{qn}$ is a zero of $\tilde{D}_{11}(\mathbf{q}, \omega)$, and the $O(N)$ scaling holds in the vicinity of this zero, $|\omega - \epsilon_{qn}| \ll n_c/N$, where the polarization operator is dominated by the contribution from the n th band spinon [see Eq. (113)]. As a result, $d\tilde{D}_{11}(\mathbf{q}, \omega)/d\omega|_{\omega=\epsilon_{qn}} \propto N$ as illustrated in Fig. 5. For $|\omega - \epsilon_{qn}| \gg n_c/N$, $D(\mathbf{q}, \omega)$ recovers the usual scaling $D(\mathbf{q}, \omega) \propto N^0$. A similar analysis shows that $\tilde{D}_{1, \sigma' > 1}$ and $\tilde{D}_{\sigma > 1, 1}$ have the same anomalous large- N scaling in the vicinity of $\omega = \epsilon_{qn}$, while the other components $\tilde{D}_{\sigma > 1, \sigma' > 1}$ satisfy the usual scaling $\tilde{D} \propto N^0$.

2. Cancellation of single-spinon poles

By using the result in Eq. (117), the bilinear form Eq. (109) can be expressed as

$$\|\tilde{\mathbf{f}}^Q(n, \mathbf{q})\| \|\mathbf{f}^Q(n, \mathbf{q})\| \tilde{D}_{11}(\mathbf{q}, \epsilon_{qn}) + O(\eta^2) \quad (118)$$

and

$$\begin{aligned} Z_{\text{FL}}^{\mu\nu}(n, \mathbf{q}) &= \frac{1}{-i\eta N} g_\mu^Q(n, \mathbf{q}) \overline{g_\nu^Q(n, \mathbf{q})} \\ &\times \|\tilde{\mathbf{f}}^Q(n, \mathbf{q})\| \|\mathbf{f}^Q(n, \mathbf{q})\| \tilde{D}_{11}(\mathbf{q}, \epsilon_{qn}). \end{aligned} \quad (119)$$

The key observation is that the residue $Z_{\text{FL}}^{\mu\nu}(n, \mathbf{q})$ is of order $1/N^0$, although it represents a (singular) contribution to a $1/N$ correction of the dynamical spin susceptibility that is diagrammatically represented in Fig. 4. We note that this anomaly arises from the first term of Eq. (117): the propagator $D(\mathbf{q}, \omega)$, which is nominally of order $1/N^0$, has a contribution of order N that is proportional to η . According to Eqs. (117) and (119), we have

$$Z_{\text{FL}}^{\mu\nu}(n, \mathbf{q}) = -g_\mu^Q(n, \mathbf{q}) \overline{g_\nu^Q(n, \mathbf{q})}. \quad (120)$$

In other words, the anomalous scaling of $Z_{\text{FL}}^{\mu\nu}(n, \mathbf{q})$ leads to an exact cancellation with the residue of $\chi_{\text{SP}}^{\mu\nu}(\mathbf{q}, \omega)$ at $\omega = \epsilon_{qn}$ that is given in Eq. (85):

$$Z_{\text{FL}}^{\mu\nu}(n, \mathbf{q}) = -Z_{\text{SP}}^{\mu\nu}(n, \mathbf{q}), \quad (121)$$

or

$$\lim_{\omega \rightarrow \epsilon_{qn}} (\epsilon_{qn} - \omega) \chi_{\text{FL}}^{\mu\nu}(\mathbf{q}, \omega) = - \lim_{\omega \rightarrow \epsilon_{qn}} (\epsilon_{qn} - \omega) \chi_{\text{SP}}^{\mu\nu}(\mathbf{q}, \omega). \quad (122)$$

Equation (121) is one of the key results of this work, which has a clear physical meaning: single-spinon excitations are not true quasiparticles of the magnetically ordered state. The true collective modes are magnons, which arise from the poles of the RPA propagator $D(\mathbf{q}, \omega)$. As we will discuss below, this important result implies that adding *all the diagrams* up to a given *nominal* order in $1/N$ is not the correct strategy to obtain qualitatively correct results in the presence of a condensate. For each diagram of a given order in $1/N$, there is a ‘‘counterdiagram’’ of higher nominal order, which must be added to cancel the unphysical single-spinon poles.

Finally, the diagram shown in Fig. 4(a6) contributes to the static and uniform magnetic susceptibility:

$$\begin{aligned} \chi_{\text{FL};(a6)}^{\mu\nu}(\mathbf{q}, \omega) &= \chi_{\text{SP};d}^{\mu\nu}(\mathbf{q}, \omega) \sum_{\alpha_1 \alpha_2} D_{\alpha_1 \alpha_2}(\mathbf{0}, \omega) f_{\alpha_1}^Q(n, \mathbf{0}) f_{\alpha_2}^Q(n, \mathbf{0}) \\ &\times \frac{\mathcal{N}_S}{2N} \left(\frac{1}{2\epsilon_c - \omega - i\eta} + \frac{1}{2\epsilon_c + \omega + i\eta} \right), \end{aligned} \quad (123)$$

where $\epsilon_c \propto \mathcal{N}_S^{-1}$ is the energy of the single-spinon state where the spinons condense in the thermodynamic limit $\mathcal{N}_S \rightarrow \infty$, and $\chi_{\text{SP};d}^{\mu\nu}(\mathbf{q}, \omega)$ is given in Eq. (88). We note that the polarization operator $\Pi(\mathbf{q}, \omega)$ contains a singularity at

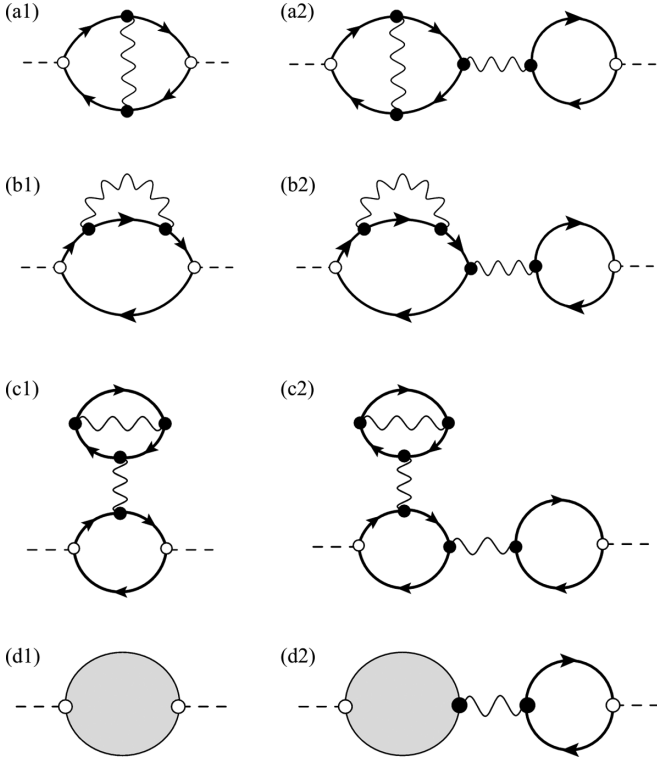


FIG. 6. Remaining diagrams of nominal order $1/N$ (a1), (b1), (c1) and their corresponding counterdiagrams (a2), (b2), (c2). (d1) Arbitrary diagram of the $1/N$ -expansion and its counterdiagram (d2). The thick solid line represents the full single-spin propagator including contributions from condensed and noncondensed spinons.

$\mathbf{q} = \mathbf{0}$ and $\omega = 2\epsilon_c$ given by Eq. (104), namely

$$\begin{aligned} \Pi_{\alpha_1\alpha_2}(\mathbf{0}, \omega) &= f_{\alpha_1}^{\mathbf{Q}}(n, \mathbf{0}) f_{\alpha_2}^{\mathbf{Q}}(n, \mathbf{0}) \frac{\mathcal{N}_s}{2N} \\ &\times \left(\frac{1}{2\epsilon_c - \omega - i\eta} + \frac{1}{2\epsilon_c + \omega + i\eta} \right) \\ &+ \text{subleading terms.} \end{aligned} \quad (124)$$

The inverse of the matrix $\Pi_0 - \Pi(\mathbf{0}, 0)$, namely the propagator $D(\mathbf{0}, 0)$, satisfies

$$\sum_{\alpha_1\alpha_2} D_{\alpha_1\alpha_2}(\mathbf{0}, 2\epsilon_c) f_{\alpha_1}^{\mathbf{Q}} f_{\alpha_2}^{\mathbf{Q}} = \frac{2N i\eta}{\mathcal{N}_s} \quad (125)$$

implying that

$$\chi_{\text{FL};(a6)}^{\mu\nu}(\mathbf{q}, \omega) = -\chi_{\text{SP};d}^{\mu\nu}(\mathbf{q}, \omega). \quad (126)$$

In other words, the (singular) SP contribution to the static and uniform magnetic susceptibility, represented by the diagram shown in Fig. 2(d), is also canceled by the diagram shown in Fig. 4(a6).

B. Self-energy and vertex corrections

The three remaining diagrams of nominal order $1/N$ that contribute to the dynamical spin susceptibility are shown in Figs. 6(a1)–6(c1). The first diagram, (a1), renormalizes the external vertex, while the other two, (b1) and (c1), renormalize the single-spin propagator. Like the saddle-point

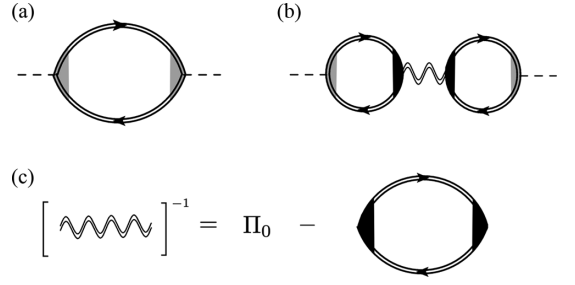


FIG. 7. (a) Magnetic susceptibility including renormalized external/internal vertices (gray/black shaded areas), spinon propagator (double solid line), and RPA propagator (double wavy line). (b) Counterdiagram that cancels out the single-spin poles of the diagram shown in panel (a). (c) Renormalized propagator of the fluctuation fields.

contribution to the magnetic susceptibility shown in Fig. 2, and the $1/N$ contribution shown in Fig. 4, these diagrams have poles at the *bare* single-spin frequencies that must be canceled by higher-order counterdiagrams. By following exactly the same procedure that we used to demonstrate that the $1/N$ contribution shown in Fig. 4 is a counterdiagram for the saddle-point contribution shown in Fig. 2, we can demonstrate that the counterdiagrams shown in Figs. 6(a2)–6(c2) cancel the single-spin poles of the contributions (a1), (b1), and (c1). In general, the counterdiagram of any diagram that has poles at the bare single-spin frequencies is constructed by simply adding the “tail” shown in Fig. 6(d2). It is interesting to note that exactly the same procedure must be followed (even in the absence of the condensate) to construct the counterdiagram that cancels the SB density fluctuations [2]. In other words, the same counterdiagram simultaneously eliminates two unphysical effects: the residues of the single-spin poles and density fluctuations that violate the constraint Eq. (2). As we discuss below, this qualitative improvement in the dynamical spin susceptibility also leads to a significant quantitative improvement, which manifests in different aspects of the theory, such as the sum rule or the sensitivity of the results to the choice of α , which are discussed in the next section.

For more general diagrams contributing to the magnetic susceptibility that include renormalized external/vertex functions and propagators of the spinon and the fluctuation fields, we can also construct counterdiagrams that cancel the *renormalized* single-spin poles. The renormalized magnetic susceptibility is generally represented by the diagram shown in Fig. 7(a). Once again, we can extend the previous derivation to demonstrate that the counterdiagram of the renormalized bubble is obtained by adding the renormalized tail shown in Fig. 7(b). The demonstration is formally the same as the one given above in the absence of vertex or self-energy renormalizations. The basic difference is the inclusion of the renormalization to the single-spin Green’s function for both noncondensed and condensed spinons, which leads to different quasiparticle energy and residues in comparison with the noninteracting case [see Eqs. (73) and (74)]. By extending the previous discussion of the SP bubble diagram, we obtain a pole in the renormalized bubble diagram [Fig. 7(a)], whose residue is formally given by Eq. (85) after incorporating the single-spin renormalizations. Note that the demonstration

of the cancellation is independent of the specific form of the external and the internal vertex functions. The crucial point is that the propagator of the fluctuation field must also be renormalized, as shown in Fig. 7(c).

VII. MAGNON POLES

Along with the cancellation of the single-spinon poles, new poles emerge from the $1/N$ correction to the dynamical magnetic susceptibility. The new poles arise from the RPA propagator $D(\mathbf{q}, \omega)$ in the diagrams shown in Fig. 4 and they represent the magnons (true collective modes of the magnetically ordered ground state) as two-spinon bound states. Unlike the single-spinon dispersion, which is strongly dependent on the mean-field decoupling of the original spin Hamiltonian (i.e., on the value of α), we will demonstrate in this section that the single-magnon dispersion is much less sensitive to the mean-field decoupling. The second purpose of this section is to demonstrate that the addition of the counterdiagram shown in Fig. 4 allows us to recover the linear SWT result in the $S \rightarrow \infty$ limit.

The RPA propagator of the square lattice Heisenberg antiferromagnet takes a block diagonal form $D_{A\lambda}(\mathbf{q}, \omega) \oplus D_B(\mathbf{q}, \omega)$ that can be explained by applying a symmetry argument to the expression of the polarization operator in terms of a retarded correlation function:

$$4i\Pi_{\alpha_1\alpha_2}(\mathbf{q}, \omega) = \frac{1}{\sqrt{\mathcal{N}_S}} \sum_{\mathbf{r}} e^{-i\mathbf{q}\cdot\mathbf{r}} \times \int_{-\infty}^0 dt e^{i\omega t} \langle G_i | [\hat{\Phi}_{\mathbf{r},0}^{\alpha_1}, \hat{\Phi}_{\mathbf{0},t}^{\alpha_2}] | G_i \rangle, \quad (127)$$

where $i = 1, 2, 3$, and α refers to the components of the vector field,

$$\hat{\Phi}_{\mathbf{r},t} \equiv ((\alpha - 1)\hat{A}_{\mathbf{r},\delta}(t), (\alpha - 1)\hat{A}_{\mathbf{r},\delta}^\dagger(t), \alpha\hat{B}_{\mathbf{r},\delta}(t), -\alpha\hat{B}_{\mathbf{r},\delta}^\dagger(t), i\hat{n}_{\mathbf{r}}(t)), \quad (128)$$

and $\hat{n}_{\mathbf{r}} \equiv \hat{\mathbf{b}}_{\mathbf{r}}^\dagger \hat{\mathbf{b}}_{\mathbf{r}}$ is the spinon density operator, $\hat{A}_{\mathbf{r},\delta} \equiv \hat{A}_{\mathbf{r},\mathbf{r}+\delta}$ and $\hat{B}_{\mathbf{r},\delta} \equiv \hat{B}_{\mathbf{r},\mathbf{r}+\delta}$. The *simple* BEC ground state of the mean-field Hamiltonian, $|G_3\rangle$, is invariant under the product of a global spin rotation by an angle φ about the z -axis, $\mathcal{U}_z(\varphi)$, and a staggered gauge transformation $C(-\varphi)$, namely, $\mathcal{U}_z(\varphi)|G_3\rangle = |G_3\rangle$ with $\tilde{\mathcal{U}}_z(\varphi) = \mathcal{U}_z(\varphi)C(-\varphi)$. The gauge transformation is necessary to keep the *simple* BEC state invariant because $\mathcal{U}_z(\varphi)$ maps the macroscopically occupied single-particle state with $\mathbf{q} = \mathbf{0}$ into a condensate in a single-particle mode that is a linear combination of the $\mathbf{q} = \mathbf{0}$ and $\boldsymbol{\pi}$ modes [see Eq. (59)]. The operators $\hat{A}_{\mathbf{r},\delta}$, $\hat{A}_{\mathbf{r},\delta}^\dagger$, and $\hat{n}_{\mathbf{r}}$ remain invariant under the gauge transformation $C(\varphi)$, while the operators $\hat{B}_{\mathbf{r},\delta}$ and $\hat{B}_{\mathbf{r},\delta}^\dagger$ acquire a complex phase factor,

$$\hat{B}_{\mathbf{r},\delta}^\dagger \xrightarrow{C(\varphi)} e^{in_{\mathbf{r}}\varphi} \hat{B}_{\mathbf{r},\delta}^\dagger, \quad (129)$$

implying that, for instance,

$$\begin{aligned} \langle G_i | \hat{A}_{\mathbf{0},\delta}^\dagger \hat{B}_{\mathbf{r},\delta}^\dagger | G_i \rangle &= \langle G_i | \tilde{\mathcal{U}}_z^\dagger(\varphi) \hat{A}_{\mathbf{0},\delta}^\dagger \hat{B}_{\mathbf{r},\delta}^\dagger \tilde{\mathcal{U}}_z(\varphi) | G_i \rangle \\ &= e^{in_{\mathbf{r}}\varphi} \langle G_i | \hat{A}_{\mathbf{0},\delta}^\dagger \hat{B}_{\mathbf{r},\delta}^\dagger | G_i \rangle. \end{aligned}$$

Then the cross-correlation function between the \hat{A} or \hat{n} and \hat{B} operators must be zero, and the propagator matrix has the form $D(\mathbf{q}, \omega) = D_{A\lambda}(\mathbf{q}, \omega) \oplus D_B(\mathbf{q}, \omega)$.

The propagator $D_{A\lambda}$ includes a zero-energy mode for each ω and \mathbf{q} value because of the redundant gauge degree of freedom [the zero mode corresponds to a gauge transformation $b_{i\sigma}(\tau) \rightarrow b_{i\sigma}(\tau)e^{i\theta_i(\tau)}$]. This unphysical mode does not contribute to any physical observable. $D_{A\lambda}$ does not have isolated poles. By contrast, the propagator of the B -fields, D_B , includes a pole singularity that becomes gapless at $\mathbf{q} = \mathbf{0}$ and $\boldsymbol{\pi}$. As we will see below, these poles represent the two Goldstone modes (transverse magnons) at $\mathbf{q} = \mathbf{0}$ and $\boldsymbol{\pi}$ expected for *collinear* magnetic ordering (it breaks two continuous spin rotation symmetries). Let us consider now the dynamical magnetic susceptibility with the correction depicted in Fig. 4. As we explained in the previous section, we only include the diagrams shown in Figs. 4(a1)–4(a6), a subset of the nominal $1/N$ diagrams, because they are the counterdiagram of the SP contribution shown in Fig. 2. Explicitly, the $1/N$ correction shown in Fig. 4 is given by

$$\chi_{\text{FL}}^{\mu\nu}(\mathbf{q}, \omega) = \sum_{\alpha_1\alpha_2} \Lambda^{\mu\alpha_1}(\mathbf{q}, \omega) \frac{1}{N} D_{\alpha_1\alpha_2}(\mathbf{q}, \omega) \Lambda^{\nu\alpha_2}(-\mathbf{q}, -\omega), \quad (130)$$

where

$$2i\Lambda^{\mu\alpha}(\mathbf{q}, \omega) = \frac{1}{\sqrt{\mathcal{N}_S}} \sum_{\mathbf{r}} e^{-i\mathbf{q}\cdot\mathbf{r}} \int_{-\infty}^0 dt e^{i\omega t} \langle G_i | [\hat{S}_{\mathbf{r},0}^\mu, \hat{\Phi}_{\mathbf{0},t}^\alpha] | G_i \rangle \quad (131)$$

is the cross susceptibility between the spin operator $\hat{S}_{\mathbf{r}}^\mu$ and the fluctuation field component $\hat{\Phi}_{\mathbf{r},t}^\alpha$ at the SP level.

Since $|G_1\rangle$ and the bond operators are invariant under global spin SU(2) spin rotations, while the spin operators transform like vectors, the cross susceptibility $\Lambda^{\mu\alpha}(\mathbf{q}, \omega)$ is equal to zero, implying that $\chi_{\text{FL}}^{\mu\nu}(\mathbf{q}, \omega) = 0$ for the isotropic SP solution $|G_1\rangle$.

The SP solution $|G_2\rangle$ is only invariant under the residual U(1) symmetry subgroup of global rotations $\mathcal{U}_z(\varphi)$ along the z -axis (direction of the ordered moments). The transverse spin components $\hat{S}_{\mathbf{r}}^\pm = \hat{S}_{\mathbf{r}}^x \pm i\hat{S}_{\mathbf{r}}^y$ acquire a complex phase $\exp(\pm i\varphi)$ under these rotations. Consequently, we still obtain that $\langle G_2 | \hat{S}_{\mathbf{r}}^\pm \hat{\Phi}_{\mathbf{0}}^\alpha | G_2 \rangle = 0$, implying that $\Lambda^{\mu\alpha}(\mathbf{q}, \omega) = 0$ and $\chi_{\text{FL}}^{\mu\nu}(\mathbf{q}, \omega) = 0$ for the transverse components $\mu, \nu = x, y$. In addition, the invariance of $|G_2\rangle$ under the gauge transformation $C(\varphi)$ implies that $\langle G_2 | \hat{S}_{\mathbf{r}}^z \hat{B}_{\mathbf{0},\delta}^\dagger | G_2 \rangle = 0$. On the one hand, since the poles of the RPA propagator arise from the B -sector (D_B), the longitudinal susceptibility does not acquire new poles after adding the correction due to fluctuations. On the other hand, the finite correction due to the nonzero cross-correlation function between $\hat{S}_{\mathbf{r}}^z$ and the A - λ fields leads to the cancellation of the single-spinon poles of the SP contribution $\chi_{\text{SP}}^{\mu\nu}(\mathbf{q}, \omega)$. This is the qualitatively correct result for the longitudinal component of the spin susceptibility for the collinear antiferromagnet under consideration (magnons are transverse modes).

The situation is qualitatively different for the simple condensate $|G_3\rangle$, as is revealed by the following symmetry argument. $|G_3\rangle$ is invariant under the residual U(1) symmetry group of global spin rotations about the z -axis

up to a gauge transformation: $\tilde{\mathcal{U}}_z(\varphi) = \mathcal{U}_z(\varphi)C(-\varphi)$ and $\tilde{\mathcal{U}}_z(\varphi)|G_3\rangle = |G_3\rangle$, implying that $\langle G_3|\hat{S}_r^z\hat{B}_{0,\delta}^\dagger|G_3\rangle = 0$ because \hat{S}_r^z is invariant under that transformation, while $\hat{B}_{0,\delta}^\dagger$ acquires a phase factor [see Eq. (129)]. In addition, $\langle G_3|\hat{S}_r^\pm\hat{\Phi}_0^\alpha|G_3\rangle = 0$ for $\hat{\Phi}^\alpha = \hat{A}, \hat{A}^\dagger, \hat{n}$ because these operators are invariant under $\tilde{\mathcal{U}}_z$, while the transverse spin components \hat{S}_r^\pm acquire a phase. Importantly, for the transverse channel, the phase factor acquired by \hat{S}_r^\pm due to the global spin rotation $\mathcal{U}_z(\varphi)$ is compensated by the phase factor acquired by $\hat{B}_{0,\delta}^\dagger$ due to the gauge transformation $C(-\varphi)$, allowing for a nonzero value of $\Lambda^{\mu\alpha}$. Consequently, the simple BEC SP solution $|G_3\rangle$ is the only one that has a finite correction due to fluctuations (diagram of Fig. 4) to the transverse components of the susceptibility: $\chi_{\text{FL}}^{\mu\nu}(\mathbf{q}, \omega) \neq 0$ for $\mu, \nu = x, y$. In summary, $\Lambda^{\mu\alpha}$ remains finite both for the longitudinal and for the transverse components. In particular, the longitudinal z component of the spin has a finite cross-correlation function with the A - λ fields, while the transverse spin components have a finite cross-correlation function with the B fields. The pole of the RPA propagator D_B gives rise to a δ -peak in the transverse spin channel of the DSSF, while the correction due to fluctuations in the longitudinal channel cancels out the poles of $\chi_{\text{SP}}^{zz}(\mathbf{q}, \omega) \neq 0$ and leaves a two-spinon continuum associated with the branch-cut singularity of $D_{A\lambda}$, which is the qualitatively correct result.

This qualitative distinction between $|G_2\rangle$ and $|G_3\rangle$ holds true for any collinear antiferromagnet revealing that the simple condensate $|G_3\rangle$ provides a more adequate description of the magnetically ordered state because a finite contribution from the fluctuations in the transverse channel is essential to cancel out the single-spinon poles of the SP contribution for $\alpha \neq 0$.

The spectral weight of the two-spinon continuum vanishes in the $S \rightarrow \infty$ limit, and the spectral weight of the DSSF is restricted to the δ -peak associated with the single pole in the transverse spin channel (magnon modes). As for the triangular lattice case [38], the dispersion and the spectral weight of these magnons become identical to the linear SWT result in that limit (see Fig. 8). Moreover, the recovery of the linear SWT result in the large- S limit is independent of the mean-field decoupling of the original spin Hamiltonian, i.e., of the choice of α in Eq. (8).

Figure 9 shows the *transverse* DSSF along high-symmetry directions for different values of α , i.e., different decoupling schemes that lead to different simple BEC SP solutions. The upper panels correspond to the SP result, while the lower panels include the contribution from the counterdiagram depicted in Fig. 4. As we explained above, the contribution from the counterdiagram vanishes for $\alpha = 0$ because of the lack of B -fields in that particular decoupling scheme. In this particular and fortuitous case, the single-spinon dispersion coincides with the single-magnon dispersion: $\varepsilon_q = \omega_q$. The situation is very different for finite values of α , where the presence of B -fields leads to the above-mentioned cancellation of the single-spinon poles of the SP solution and to the emergence of new magnon poles arising from the fluctuation of the B -fields. It is interesting to note that the bandwidth of the single-spinon dispersion (poles of the SP solution) decreases by a factor of 2 when α evolves from zero to 0.5 [see Figs. 9(a)–9(c)].

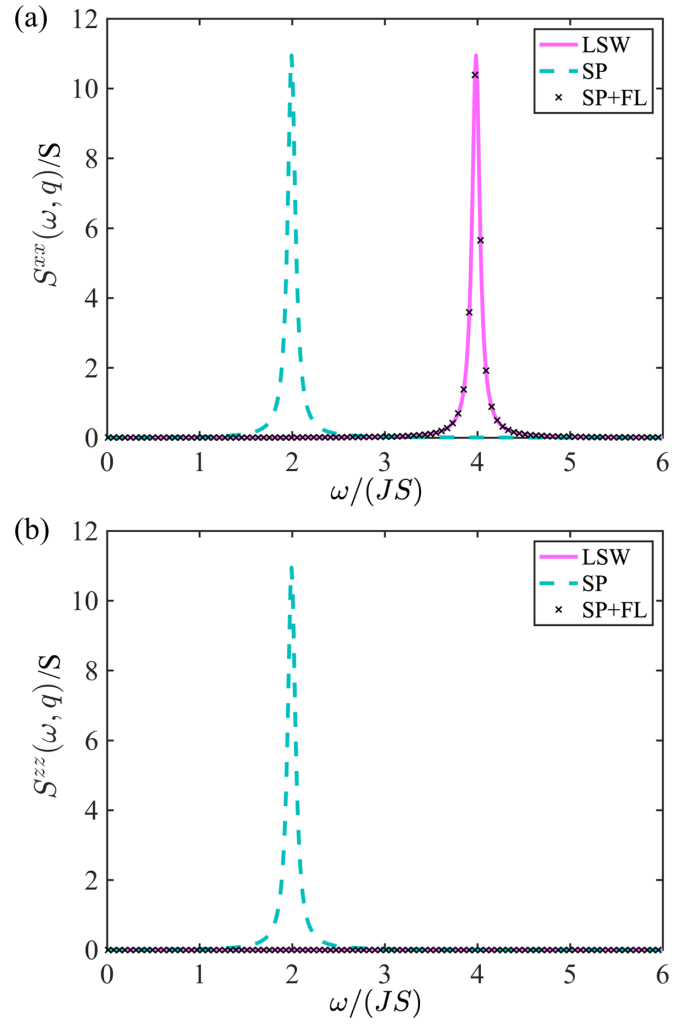


FIG. 8. Recovery of semiclassical limit ($S \rightarrow \infty$) with the Schwinger boson theory by including fluctuations around the SP solution $|G_3\rangle$ for a decoupling parameter $\alpha = 0.5$. Transverse (a) and longitudinal (b) DSSF for an arbitrarily chosen momentum $\mathbf{q} = (1.25, 2.09)$ in r.l.u.

In contrast, the bandwidth of the single-magnon dispersion is much less dependent on α [see Figs. 9(d)–9(f)]. For instance, the energy of the magnon at $\mathbf{q} = (0, \pi)$ varies over the range [1.8, 2.316] for $0 \leq \alpha \leq 0.5$. This energy range is consistent with numerical results [84,85]. In other words, the inclusion of corrections beyond the SP makes the final result less sensitive to the choice of the SP. Nevertheless, there is still a significant α -dependence of the magnon spectral weight and the distribution of the two-spinon continuum, implying that for low-order expansions in $1/N$ it is necessary to introduce a criterion for choosing an optimal decoupling scheme (value of α). In particular, note that some magnons are overdamped above a critical value of α because they overlap with the two-spinon continuum [e.g., the magnons modes with energy $\sim 2J$ along the path $(\pi/2, \pi/2)$ – $(\pi, 0)$ shown in Figs. 9(e)–9(g)].

For the *longitudinal* component of the DSSF, shown in Fig. 10, the main difference between the SP result (upper row) and the one that includes the contribution from the counterdiagram shown in Fig. 4 is that the latter (lower row) has

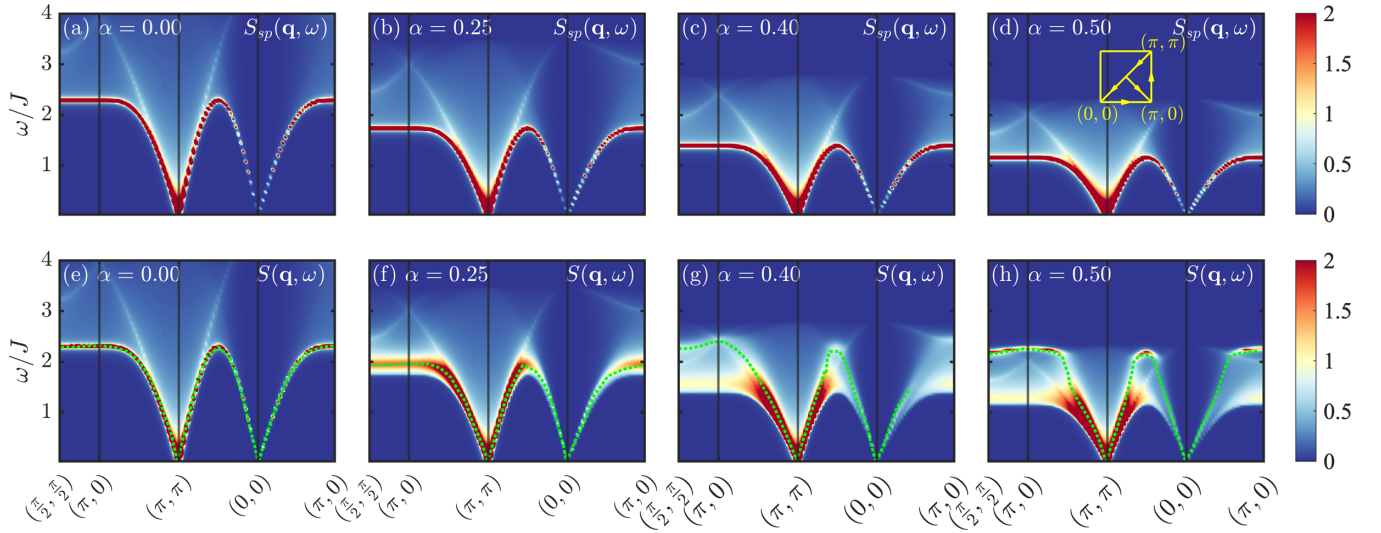


FIG. 9. Transverse dynamical spin structure factor ($S = 1/2$). Parts (a)–(d) show the SP result for the simple BEC solution represented by the state $|G_3\rangle$ and $\alpha = 0, 0.25, 0.4, 0.5$, while (e)–(h) include the $1/N$ correction described in Fig. 4. Note that $S^{xx}(\mathbf{q}, \omega) = S^{yy}(\mathbf{q}, \omega)$. The green dots indicate the magnon dispersion. Inset: high-symmetry path of the horizontal axis.

no poles. As we already explained, the lack of poles in the longitudinal channel is the qualitatively correct result. It is also important to note that the distribution of spectral weight in the two-spinon continuum is still strongly dependent on α . This is a direct consequence of the α -dependence of the single-spinon dispersion at the SP level: $\varepsilon_q = (1 - \alpha)\omega_q$. To make this result less sensitive to α , it is necessary to renormalize the single-spinon propagator by including diagrams such as the ones shown in Figs. 6(b1) and 6(c1). This renormalization is also expected to account for many-body effects that are not captured at the current level of approximation. For instance, it is well known that the hybridization between single- and three-magnon states leads to a rotonlike anomaly in the single-magnon dispersion at $\mathbf{q} = (0, \pi)$ or $\mathbf{q} = (\pi, 0)$ [84–88]. Since magnons are obtained as two-spinon

bound states in the SBT, few-body effects caused by three-magnon states will manifest via hybridization between the two-spinon and six-spinon sectors (note that the renormalization of the single-spinon propagator will in turn renormalize the RPA propagator and its poles).

Figure 11 shows the trace of the DSSF (transverse plus longitudinal components) for different values of α . As we anticipated in Sec. IV, the exact sum rule $\int d\omega d^3q S(\mathbf{q}, \omega) = \mathcal{N}_s S(S + 1)$ provides a good test for any approximation scheme. According to Eq. (71), the SP result overestimates the sum rule by $\approx 50\%$. In contrast, the integration of the total dynamical spin structure factor, shown in Fig. 12, gives $\int d\omega d^3q S(\mathbf{q}, \omega) = \mathcal{N}_s \zeta(\alpha) S(S + 1)$, with $\zeta(0) \approx 1.133$ and $\zeta(0.5) \approx 1.125$. To obtain these results, we computed the integral of $S(\mathbf{q}, \omega)$ for different values of η (Lorentzian broad-

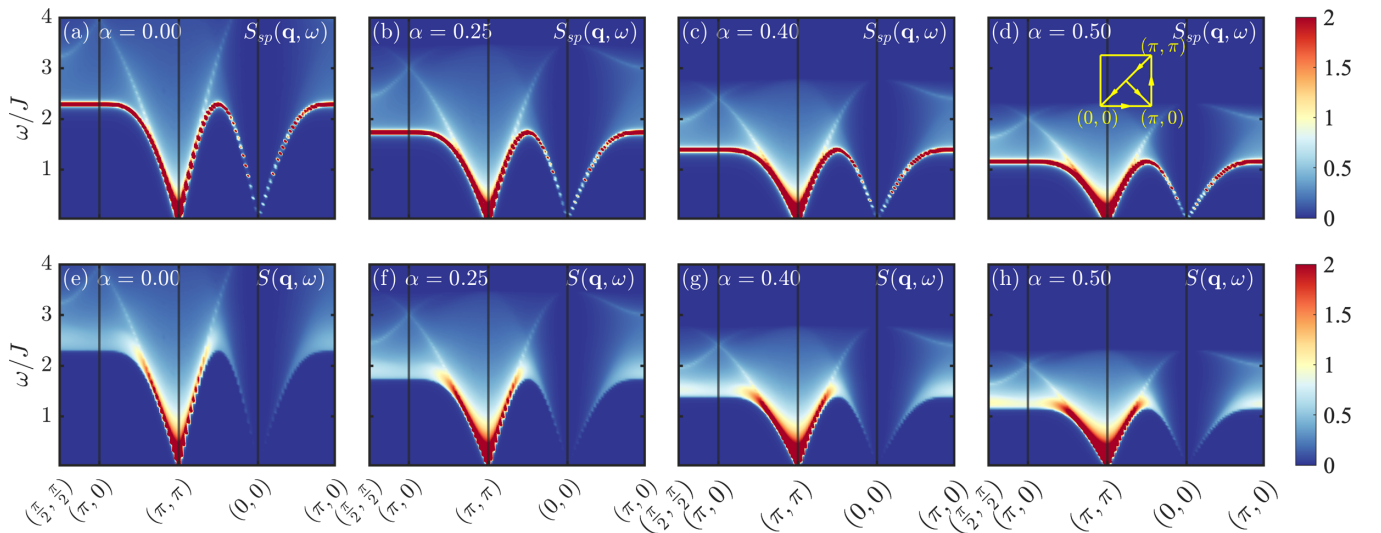


FIG. 10. Longitudinal dynamical spin structure factor ($S = 1/2$). Parts (a)–(d) show the SP result for the simple BEC solution represented by the state $|G_3\rangle$ and $\alpha = 0, 0.25, 0.4, 0.5$, while (e)–(h) include the $1/N$ correction described in Fig. 4. Inset: high-symmetry path of the horizontal axis.

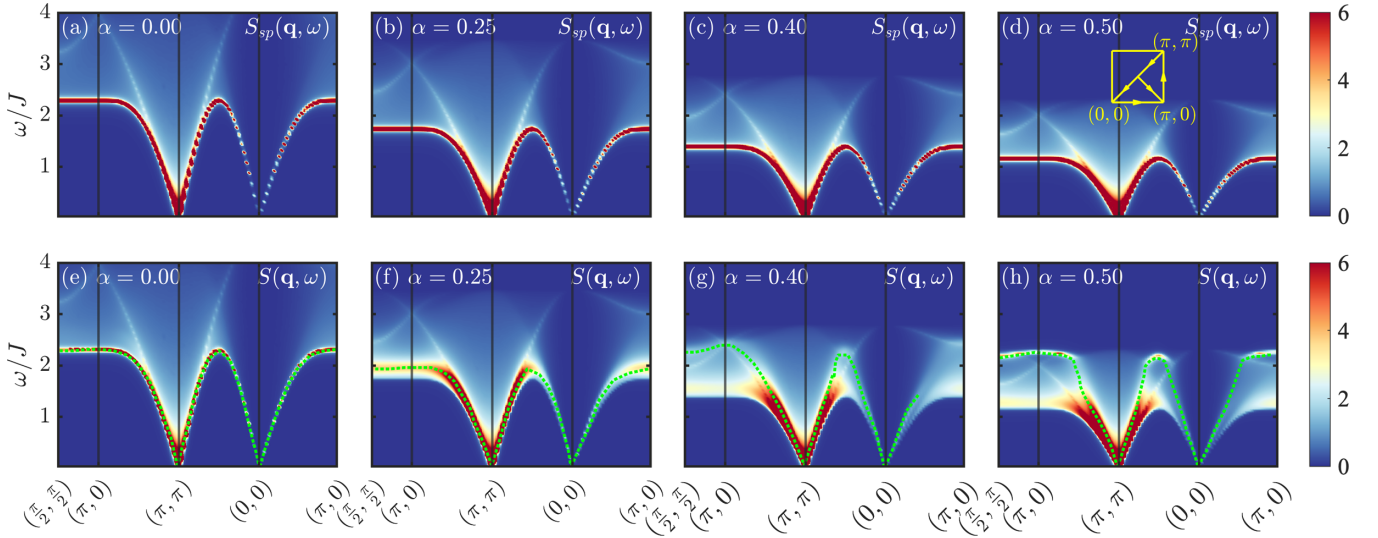


FIG. 11. Total dynamical spin structure factor $S(\mathbf{q}, \omega) = \sum_{\mu} S^{\mu\mu}(\mathbf{q}, \omega)$ ($S = 1/2$). Parts (a)–(d) show the result for the SP solution $|G_3\rangle$ and $\alpha = 0, 0.25, 0.4, 0.5$, and (e)–(h) include the $1/N$ correction described in Fig. 4. The green dots indicate the magnon dispersion. Inset: high-symmetry path of the horizontal axis.

ening) and for system sizes $\mathcal{N}_s = 144, 576$, and 1024 . We then performed a linear extrapolation in the width $\eta \rightarrow 0$ [see Figs. 12(a)–12(c)] for each system size, and the result was in turn extrapolated to the thermodynamic limit $1/\mathcal{N}_s \rightarrow 0$. As is clear from Fig. 12, the sum rule exhibits a very weak dependence on $1/\mathcal{N}_s$ and η for small enough values of these parameters. As is shown in Fig. 12(e), the value of $\zeta(\alpha)$ for intermediate values of α , $0 < \alpha < 0.5$, is well approximated by a linear interpolation between the above-mentioned extreme values. Clearly, the sum rule remains basically independent of the decoupling scheme, and the inclusion of the new contribution produces a much better approximation to the exact sum

rule. Since violations of the sum rule arise from violations of the physical constraint Eq. (2), we confirm that the addition of the counterdiagram shown in Fig. 4 also leads to a much better approximation of the local constraint.

Finally, we should say a few words about the criterion that must be adopted to determine the “optimal” decoupling scheme, i.e., the value of α . In the past, different groups have used comparisons of the ground-state energy against exact diagonalization results on finite-size clusters to discriminate between different decoupling schemes [7,14,20,22,89–91]. An alternative criterion could be to directly compare the DSSF against results obtained on finite-size clusters or from

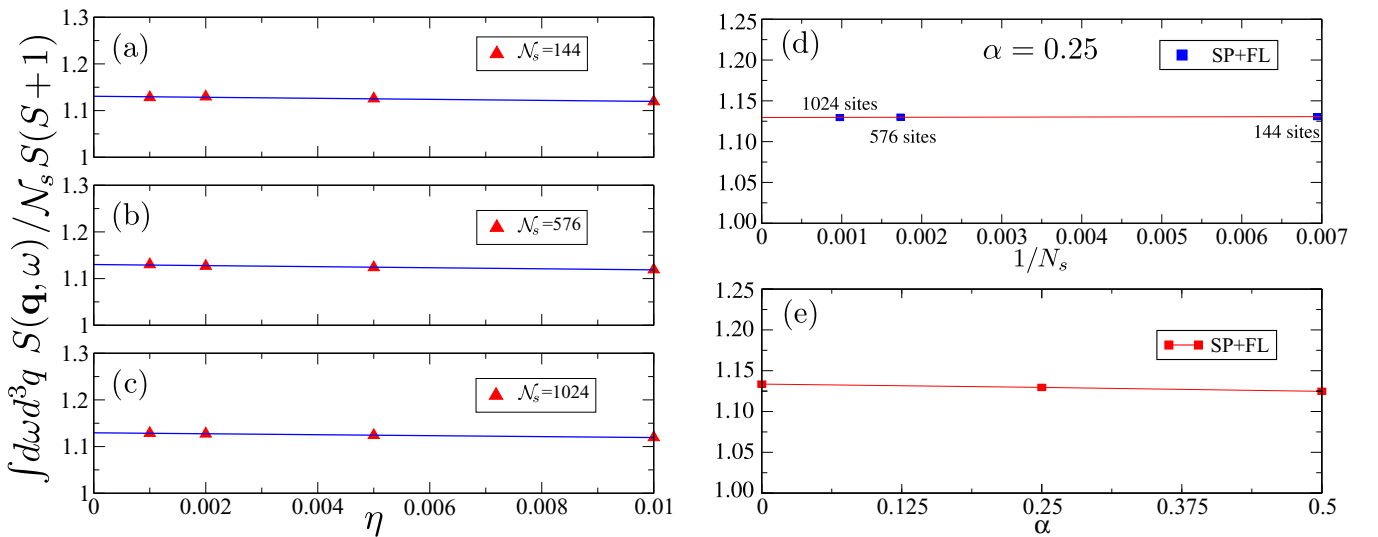


FIG. 12. Linear extrapolation of the integral over frequency and momentum of the dynamical spin structure factor after correcting the simple BEC SP result [see Eq. (71)] with the contribution described in Fig. 4. The panels (a)–(c) correspond to extrapolations as a function of the width η for $\alpha = 0.25$ and finite lattices of $\mathcal{N}_s = 144, 576$, and 1024 , respectively. Panel (d) shows the finite-size scaling and the extrapolation to the thermodynamic limit of the extrapolated ($\eta \rightarrow 0$) results obtained in the previous panels. Panel (e) shows the final result after performing the $\eta \rightarrow 0$ and $\mathcal{N}_s \rightarrow \infty$ extrapolations for different values of α .

experiments. This criterion has been applied to the triangular lattice antiferromagnet obtaining an optimal value of α close to 0.5 [37,38].

VIII. SUMMARY

As we already mentioned in the Introduction, most attempts at using the SBT to describe magnetically ordered systems have not gone beyond the saddle-point level. In this work, we have presented a comprehensive approach to the selection of the magnetically ordered SP solution and inclusion of higher-order corrections of the $1/N$ expansion. As we argued in the previous sections, the presence of a condensate associated with the magnetic ordering generates multiple subtleties that have been omitted in previous discussions of the SBT. The main motivation of this work has not been to solve again the particular case of the square lattice antiferromagnet, but to employ this textbook model to illustrate how a proper choice of the SP solution and a careful analysis of the cancellations that occur in the presence of a condensate can improve the results both qualitatively and quantitatively.

On the one hand, we have carefully examined the consequences of the freedom associated with the choice of the decoupling scheme (value of α) and the fragmented versus simple nature of the BEC ground state of the SP Hamiltonian for a fixed value of α . On the other hand, we have seen that Feynman diagrams, which in the absence of the condensate would contribute to a given order in $1/N$, acquire singular lower-order contributions in the presence of a condensate. Upon expanding the dynamical spin susceptibility in powers of $1/N$, these singular contributions lead to the existence of counterdiagrams that exactly cancel out the residues of the single-spinon poles of a given diagram, as expected for the excitation spectrum of magnetically ordered states. The true quasiparticles of the ordered system are then magnons or transverse modes that to the lowest nontrivial order in $1/N$ arise from poles of the RPA propagator. Correspondingly, a main conclusion of this work is that in a correct expansion of the magnetic susceptibility of an ordered magnet, *each diagram must be accompanied by its counterdiagram*.

Among other consequences, this important conclusion implies that it is strictly necessary to go beyond the SP level to obtain physically correct results for magnetically ordered systems. In other words, the loop diagram depicted in Fig. 2, which is the SP contribution to the dynamical spin susceptibility, must be accompanied by its counterdiagram depicted in Fig. 6, which is *nominally* of order $1/N$. This requirement was first noticed (without a clear justification) in a previous work on the triangular Heisenberg antiferromagnet [37]. The reason why this subtle point remained hidden for approximately 30 years is that the SBT was first applied to the square lattice Heisenberg antiferromagnet [1,7]. As we discussed in the previous section, the AA or $\alpha = 0$ decoupling scheme that was originally applied to the square lattice Heisenberg antiferromagnet [1,7] has an important peculiarity: the single-spinon dispersion coincides with the single-magnon dispersion, and the contribution from the counterdiagram vanishes *for the transverse* dynamical spin susceptibility. This “pathology” of the particular case $\alpha = 0$ led the community to believe that the SP level of the SBT is enough to obtain the true

collective modes of magnetically ordered states. While this generalized belief was questioned after noticing the impossibility of recovering the correct large- S limit with the SP result for the general case (noncollinear orderings) [75,76], the origin of this failure was not properly understood. As we have demonstrated here, the identity between the single-spinon and single-magnon dispersions is not true for general decoupling schemes ($\alpha \neq 0$). Moreover, the pathology is completely absent in systems with noncollinear magnetic ordering, such as the triangular lattice AFM. As was demonstrated in a previous work [38], the addition of the counterdiagram allows us to recover the correct result in the large- S limit. Furthermore, as was shown in this work, *this result is independent of the decoupling scheme parametrized by α* .

Another subtlety of the SBT applied to the square lattice Heisenberg antiferromagnet is related to the freedom associated with the choice of the spinon condensate in the presence of a symmetry-breaking field. This freedom arises from the collinear nature of the antiferromagnetic ordering that leads to a U(1) residual symmetry group for SU(2)-invariant Heisenberg interactions. While the symmetry-breaking field polarizes the condensed spinons along the field direction in the twisted reference frame, the spinons can still condense in more than one gapless mode ($\mathbf{q} = \mathbf{0}$ or $\mathbf{q} = \boldsymbol{\pi}$ for a particular gauge choice of the square lattice antiferromagnet SBT considered here). This remaining ground-state degeneracy of the SP Hamiltonian introduces more freedom in the choice of the condensate. As we have seen in Sec. IV, the importance of choosing a “simple” spinon BEC instead of the fragmented BEC adopted in previous works [2] becomes evident after including corrections beyond the SP level. Furthermore, if we continuously deform the triangular lattice antiferromagnet into the square lattice Heisenberg antiferromagnet, the *unique* BEC solution of the noncollinear triangular antiferromagnet evolves continuously into the simple BEC solution of the square lattice antiferromagnet.

By considering all the above-mentioned subtleties, we have finally shown that including corrections beyond the SP level is crucial not only to reveal the true quasiparticles of the magnetically ordered state, but also to reduce the dependence of the dynamical spin susceptibility on the decoupling scheme (value of α). We note, however, that the two-spinon continuum is still strongly dependent on α because we have not included the diagrams shown in Figs. 6(b1) and 6(c1) that renormalize the single-spinon propagator. A natural consequence of this limitation of the current level of approximation is that some magnon modes become overdamped above a critical value of α because they overlap with the two-spinon continuum. We expect that this undesirable result will be corrected after including a proper renormalization of the single-spinon propagator. A detailed study of the different effects of the single-spinon renormalization will be the subject of future work. Based on the preliminary results presented in this work, we conclude that the optimal decoupling scheme (value of α) should be determined by comparing the spectrum of low-energy excitations against some reference that can either be a numerical result on finite lattices or an experimental result.

Finally, the SBT presented here is particularly relevant for modeling magnetically ordered materials in the vicinity of a quantum critical point that signals a continuous transition

into a spin liquid state. The simple reason is that magnons become composite particles (two-spinon bound states) in the vicinity of the “quantum melting point.” The triangular lattice Heisenberg antiferromagnet [37,92] provides a natural example of this scenario because the quantum melting point is reached by adding a second-neighbor antiferromagnetic interaction that is only 6% of the nearest-neighbor exchange [55–57,62,93–95].

ACKNOWLEDGMENTS

We wish to thank A. V. Chubukov, C. Gazza, and O. Starykh for useful conversations. This work was partially supported by CONICET under Grant No. 364 (PIP2015). E.A.G. was partially supported by the LANL Directed Research and Development program. The work of C.D.B. was supported by the U.S. Department of Energy, Office of Science, Office of Basic Energy Sciences, under Award No. DE-SC0022311.

APPENDIX: RELATION FROM PARTICLE-HOLE SYMMETRY

The Nambu representation has an artificial “particle-hole” symmetry because $\psi_i = P(\psi_i^\dagger)^T$ or $\psi_q = P(\psi_{-q}^\dagger)^T$ (momentum space), where $P = \sigma_x \otimes I_0$. The invariance of the effective action under this transformation implies that the dynamical matrix satisfies $P\mathcal{M}^T(-p, -k)P^T = \mathcal{M}(k, p)$, where $k \equiv (\mathbf{k}, i\omega)$ and $p \equiv (\mathbf{p}, iv)$. The external/internal vertices are the

first derivatives of $\mathcal{M}(k, p)$ with respect to the external source term h_q^μ or the fluctuation fields $\phi_\alpha(q)$. It then follows that

$$P(u^\mu)^T P = u^\mu, \quad P[v_\alpha(\mathbf{k}, \mathbf{q})]^T P = v_\alpha(-\mathbf{q}, -\mathbf{k}). \quad (\text{A1})$$

In the SP approximation, the inverse of $\mathcal{M}(k, p) \equiv [-i\omega\gamma^0 + H_{\text{sp}}(\mathbf{k})]\delta_{k,p}$ gives rise to the single spinon’s Green’s function. We have

$$PH_{\text{sp}}^*(-\mathbf{k})P = H_{\text{sp}}(\mathbf{k}), \quad P\mathcal{G}_n(-\mathbf{k}, -\omega)^T P = \mathcal{G}_n(\mathbf{k}, \omega). \quad (\text{A2})$$

The eigenstates of the SP Hamiltonian must then satisfy the relations

$$X_{\mathbf{k},\alpha} = P\bar{X}_{-\mathbf{k},\alpha}^*, \quad \bar{X}_{\mathbf{k},\alpha} = PX_{-\mathbf{k},\alpha}^*. \quad (\text{A3})$$

In particular, the eigenstate $|c_Q\rangle \equiv X_{\mathbf{Q},+1}$ or $\bar{X}_{\mathbf{Q},+1}$ (identical in the thermodynamic limit) satisfies

$$|c_Q\rangle = P(|c_Q\rangle)^*, \quad (\text{A4})$$

where we have assumed that $\mathbf{Q} = -\mathbf{Q}$ is an inversion-invariant momentum vector.

Using Eqs. (A1)–(A4), we can show that the two diagrams in Figs. 2(b) and 2(c) are equal to each other. For instance, their contributions to the DSSF, Eqs. (79) and (82), are identical. A similar conclusion holds in the calculation of the other diagrams in this work.

-
- [1] D. P. Arovas and A. Auerbach, Functional integral theories of low-dimensional quantum Heisenberg models, *Phys. Rev. B* **38**, 316 (1988).
- [2] A. Auerbach, *Interacting Electrons and Quantum Magnetism* (Springer Science & Business Media, 2012).
- [3] J. E. Hirsch and S. Tang, Comment on a mean-field theory of quantum antiferromagnets, *Phys. Rev. B* **39**, 2850 (1989).
- [4] S. Sarker, C. Jayaprakash, H. R. Krishnamurthy, and M. Ma, Bosonic mean-field theory of quantum Heisenberg spin systems: Bose condensation and magnetic order, *Phys. Rev. B* **40**, 5028 (1989).
- [5] P. Chandra, P. Coleman, and A. I. Larkin, A quantum fluids approach to frustrated Heisenberg models, *J. Phys.: Condens. Matter* **2**, 7933 (1990).
- [6] N. D. Mermin and H. Wagner, Absence of Ferromagnetism or Antiferromagnetism in One- or Two-Dimensional Isotropic Heisenberg Models, *Phys. Rev. Lett.* **17**, 1133 (1966).
- [7] A. Auerbach and D. P. Arovas, Spin Dynamics in the Square-Lattice Antiferromagnet, *Phys. Rev. Lett.* **61**, 617 (1988).
- [8] N. Read and S. Sachdev, Valence-Bond and Spin-Peierls Ground States of Low-Dimensional Quantum Antiferromagnets, *Phys. Rev. Lett.* **62**, 1694 (1989).
- [9] N. Read and S. Sachdev, Spin-Peierls, valence-bond solid, and Néel ground states of low-dimensional quantum antiferromagnets, *Phys. Rev. B* **42**, 4568 (1990).
- [10] N. Read and S. Sachdev, Large-N Expansion for Frustrated Quantum Antiferromagnets, *Phys. Rev. Lett.* **66**, 1773 (1991).
- [11] S. Sachdev and N. Read, Large N expansion for frustrated and doped quantum antiferromagnets, *Int. J. Mod. Phys. B* **05**, 219 (1991).
- [12] F. Mila, D. Poilblanc, and C. Bruder, Spin dynamics in a frustrated magnet with short-range order, *Phys. Rev. B* **43**, 7891 (1991).
- [13] S. Sachdev, Kagomé and triangular-lattice Heisenberg antiferromagnets: Ordering from quantum fluctuations and quantum-disordered ground states with unconfined bosonic spinons, *Phys. Rev. B* **45**, 12377 (1992).
- [14] H. A. Ceccatto, C. J. Gazza, and A. E. Trumper, Nonclassical disordered phase in the strong quantum limit of frustrated antiferromagnets, *Phys. Rev. B* **47**, 12329 (1993).
- [15] M. Raykin and A. Auerbach, $1/N$ expansion and spin correlations in constrained wave functions, *Phys. Rev. B* **47**, 5118 (1993).
- [16] A. V. Chubukov, S. Sachdev, and T. Senthil, Quantum phase transitions in frustrated quantum antiferromagnets, *Nucl. Phys. B* **426**, 601 (1994).
- [17] K. Lefmann and P. Hedegård, Neutron-scattering cross section of the $S=1/2$ Heisenberg triangular antiferromagnet, *Phys. Rev. B* **50**, 1074 (1994).
- [18] A. Mattsson, Spin dynamics of the triangular Heisenberg antiferromagnet: A Schwinger-boson approach, *Phys. Rev. B* **51**, 11574 (1995).
- [19] A. V. Chubukov and O. A. Starykh, Confinement of spinons in the CP^{M-1} model, *Phys. Rev. B* **52**, 440 (1995).
- [20] A. E. Trumper, L. O. Manuel, C. J. Gazza, and H. A. Ceccatto, Schwinger-Boson Approach to Quantum Spin Systems: Gaus-

- sian Fluctuations in the “Natural” Gauge, *Phys. Rev. Lett.* **78**, 2216 (1997).
- [21] C. Timm, S. M. Girvin, P. Henelius, and A. W. Sandvik, $1/N$ expansion for two-dimensional quantum ferromagnets, *Phys. Rev. B* **58**, 1464 (1998).
- [22] L. O. Manuel and H. A. Ceccatto, Magnetic and quantum disordered phases in triangular-lattice Heisenberg antiferromagnets, *Phys. Rev. B* **60**, 9489 (1999).
- [23] A. A. Burkov and A. H. MacDonald, Lattice pseudospin model for $\nu = 1$ quantum Hall bilayers, *Phys. Rev. B* **66**, 115320 (2002).
- [24] G. Misguich and C. Lhuillier, Two-dimensional quantum antiferromagnets, in *Frustrated Spin Systems* (World Scientific, Singapore, 2005), pp. 229–306.
- [25] F. Wang and A. Vishwanath, Spin-liquid states on the triangular and kagomé lattices: A projective-symmetry-group analysis of Schwinger-boson states, *Phys. Rev. B* **74**, 174423 (2006).
- [26] O. Tchernyshyov, R. Moessner, and S. L. Sondhi, Flux expulsion and greedy bosons: Frustrated magnets at large N , *Europhys. Lett.* **73**, 278 (2006).
- [27] H. Katsura, S. Onoda, J. H. Han, and N. Nagaosa, Quantum Theory of Multiferroic Helimagnets: Collinear and Helical Phases, *Phys. Rev. Lett.* **101**, 187207 (2008).
- [28] R. Flint and P. Coleman, Symplectic N and time reversal in frustrated magnetism, *Phys. Rev. B* **79**, 014424 (2009).
- [29] A. Mezio, C. N. Sposetti, L. O. Manuel, and A. E. Trumper, A test of the bosonic spinon theory for the triangular antiferromagnet spectrum, *Europhys. Lett.* **94**, 47001 (2011).
- [30] A. Mezio, L. O. Manuel, R. R. P. Singh, and A. E. Trumper, Low temperature properties of the triangular-lattice antiferromagnet: a bosonic spinon theory, *New J. Phys.* **14**, 123033 (2012).
- [31] M. Kargarian, A. Langari, and G. A. Fiete, Unusual magnetic phases in the strong interaction limit of two-dimensional topological band insulators in transition metal oxides, *Phys. Rev. B* **86**, 205124 (2012).
- [32] L. Messio, C. Lhuillier, and G. Misguich, Time reversal symmetry breaking chiral spin liquids: Projective symmetry group approach of bosonic mean-field theories, *Phys. Rev. B* **87**, 125127 (2013).
- [33] E. A. Ghioldi, A. Mezio, L. O. Manuel, R. R. P. Singh, J. Oitmaa, and A. E. Trumper, Magnons and excitation continuum in xxz triangular antiferromagnetic model: Application to $\text{Ba}_3\text{CoSb}_2\text{O}_9$, *Phys. Rev. B* **91**, 134423 (2015).
- [34] X. Yang and F. Wang, Schwinger boson spin-liquid states on square lattice, *Phys. Rev. B* **94**, 035160 (2016).
- [35] J. C. Halimeh and M. Punk, Spin structure factors of chiral quantum spin liquids on the kagome lattice, *Phys. Rev. B* **94**, 104413 (2016).
- [36] D.-V. Bauer and J. O. Fjærstad, Schwinger-boson mean-field study of the J_1 - J_2 Heisenberg quantum antiferromagnet on the triangular lattice, *Phys. Rev. B* **96**, 165141 (2017).
- [37] E. A. Ghioldi, M. G. Gonzalez, S.-S. Zhang, Y. Kamiya, L. O. Manuel, A. E. Trumper, and C. D. Batista, Dynamical structure factor of the triangular antiferromagnet: Schwinger boson theory beyond mean field, *Phys. Rev. B* **98**, 184403 (2018).
- [38] S.-S. Zhang, E. A. Ghioldi, Y. Kamiya, L. O. Manuel, A. E. Trumper, and C. D. Batista, Large- S limit of the large- N theory for the triangular antiferromagnet, *Phys. Rev. B* **100**, 104431 (2019).
- [39] Y.-D. Li, X. Yang, Y. Zhou, and G. Chen, Non-Kitaev spin liquids in Kitaev materials, *Phys. Rev. B* **99**, 205119 (2019).
- [40] X.-G. Wen, Quantum orders and symmetric spin liquids, *Phys. Rev. B* **65**, 165113 (2002).
- [41] X.-G. Wen, *Quantum Field Theory of Many-Body Systems* (Oxford University Press, Oxford, 2004).
- [42] T. Senthil, A. Vishwanath, L. Balents, S. Sachdev, and M. P. A. Fisher, Deconfined quantum critical points, *Science* **303**, 1490 (2004).
- [43] P. Ghaemi and T. Senthil, Néel order, quantum spin liquids, and quantum criticality in two dimensions, *Phys. Rev. B* **73**, 054415 (2006).
- [44] S. Sachdev, Quantum magnetism and criticality, *Nat. Phys.* **4**, 173 (2008).
- [45] B. Normand, Frontiers in frustrated magnetism, *Contemp. Phys.* **50**, 533 (2009).
- [46] L. Balents, Spin liquids in frustrated magnets, *Nature (London)* **464**, 199 (2010).
- [47] B. J. Powell and R. H. McKenzie, Quantum frustration in organic Mott insulators: from spin liquids to unconventional superconductors, *Rep. Prog. Phys.* **74**, 056501 (2011).
- [48] *Introduction to Frustrated Magnetism: Materials, Experiments, Theory*, edited by C. Lacroix, P. Mendels, and F. Mila (Springer-Verlag, Berlin, 2011).
- [49] S. Yan, D. A. Huse, and S. R. White, Spin-liquid ground state of the $S = 1/2$ kagome Heisenberg antiferromagnet, *Science* **332**, 1173 (2011).
- [50] T.-H. Han, J. S. Helton, S. Chu, D. G. Nocera, J. A. Rodriguez-Rivera, C. Broholm, and Y. S. Lee, Fractionalized excitations in the spin-liquid state of a kagome-lattice antiferromagnet, *Nature (London)* **492**, 406 (2012).
- [51] T. Li, F. Becca, W. Hu, and S. Sorella, Gapped spin-liquid phase in the $J_1 - J_2$ Heisenberg model by a bosonic resonating valence-bond ansatz, *Phys. Rev. B* **86**, 075111 (2012).
- [52] A. M. Essin and M. Hermele, Classifying fractionalization: Symmetry classification of gapped z_2 spin liquids in two dimensions, *Phys. Rev. B* **87**, 104406 (2013).
- [53] J. Merino, M. Holt, and B. J. Powell, Spin-liquid phase in a spatially anisotropic frustrated antiferromagnet: A Schwinger boson mean-field approach, *Phys. Rev. B* **89**, 245112 (2014).
- [54] Z. Zhu and S. R. White, Spin liquid phase of the $S = \frac{1}{2} J_1 - J_2$ Heisenberg model on the triangular lattice, *Phys. Rev. B* **92**, 041105(R) (2015).
- [55] W.-J. Hu, S.-S. Gong, W. Zhu, and D. N. Sheng, Competing spin-liquid states in the spin- $\frac{1}{2}$ Heisenberg model on the triangular lattice, *Phys. Rev. B* **92**, 140403(R) (2015).
- [56] Y. Iqbal, W.-J. Hu, R. Thomale, D. Poilblanc, and F. Becca, Spin liquid nature in the Heisenberg $J_1 - J_2$ triangular antiferromagnet, *Phys. Rev. B* **93**, 144411 (2016).
- [57] S. N. Saadatmand and I. P. McCulloch, Symmetry fractionalization in the topological phase of the spin- $\frac{1}{2} J_1 - J_2$ triangular Heisenberg model, *Phys. Rev. B* **94**, 121111(R) (2016).
- [58] L. Savary and L. Balents, Quantum spin liquids: a review, *Rep. Prog. Phys.* **80**, 016502 (2017).
- [59] Y. Zhou, K. Kanoda, and T.-K. Ng, Quantum spin liquid states, *Rev. Mod. Phys.* **89**, 025003 (2017).

- [60] P. Kos and M. Punk, Quantum spin liquid ground states of the Heisenberg-Kitaev model on the triangular lattice, *Phys. Rev. B* **95**, 024421 (2017).
- [61] N. Ma, G.-Y. Sun, Y.-Z. You, C. Xu, A. Vishwanath, A. W. Sandvik, and Z. Y. Meng, Dynamical signature of fractionalization at a deconfined quantum critical point, *Phys. Rev. B* **98**, 174421 (2018).
- [62] Z. Zhu, P. A. Maksimov, S. R. White, and A. L. Chernyshev, Topography of Spin Liquids on a Triangular Lattice, *Phys. Rev. Lett.* **120**, 207203 (2018).
- [63] H. Takagi, T. Takayama, G. Jackeli, G. Khaliullin, and S. E. Nagler, Concept and realization of Kitaev quantum spin liquids, *Nat. Rev. Phys.* **1**, 264 (2019).
- [64] X.-G. Wen, Choreographed entanglement dances: Topological states of quantum matter, *Science* **363**, eaal3099 (2019).
- [65] F. Ferrari and F. Becca, Dynamical Structure Factor of the $J_1 - J_2$ Heisenberg Model on the Triangular Lattice: Magnons, Spinons, and Gauge Fields, *Phys. Rev. X* **9**, 031026 (2019).
- [66] C. Broholm, R. J. Cava, S. A. Kivelson, D. G. Nocera, M. R. Norman, and T. Senthil, Quantum spin liquids, *Science* **367**, eaay0668 (2020).
- [67] F. Wang, Schwinger boson mean field theories of spin liquid states on a honeycomb lattice: Projective symmetry group analysis and critical field theory, *Phys. Rev. B* **82**, 024419 (2010).
- [68] Y. Shirata, H. Tanaka, A. Matsuo, and K. Kindo, Experimental Realization of a Spin-1/2 Triangular-Lattice Heisenberg Antiferromagnet, *Phys. Rev. Lett.* **108**, 057205 (2012).
- [69] T. Susuki, N. Kurita, T. Tanaka, H. Nojiri, A. Matsuo, K. Kindo, and H. Tanaka, Magnetization Process and Collective Excitations in the $S = 1/2$ Triangular-Lattice Heisenberg Antiferromagnet $\text{Ba}_3\text{CoSb}_2\text{O}_9$, *Phys. Rev. Lett.* **110**, 267201 (2013).
- [70] J. Ma, Y. Kamiya, T. Hong, H. B. Cao, G. Ehlers, W. Tian, C. D. Batista, Z. L. Dun, H. D. Zhou, and M. Matsuda, Static and Dynamical Properties of the Spin-1/2 Equilateral Triangular-Lattice Antiferromagnet $\text{Ba}_3\text{CoSb}_2\text{O}_9$, *Phys. Rev. Lett.* **116**, 087201 (2016).
- [71] S. Ito, N. Kurita, H. Tanaka, S. Ohira-Kawamura, K. Nakajima, S. Itoh, K. Kuwahara, and K. Kakurai, Structure of the magnetic excitations in the spin-1/2 triangular-lattice Heisenberg antiferromagnet $\text{Ba}_3\text{CoSb}_2\text{O}_9$, *Nat. Commun.* **8**, 235 (2017).
- [72] Y. Kamiya, L. Ge, T. Hong, Y. Qiu, D. Quintero-Castro, Z. Lu, H. Cao, M. Matsuda, E. S. Choi, C. Batista, M. Mourigal, H. D. Zhou, and J. Ma, The nature of spin excitations in the one-third magnetization plateau phase of $\text{Ba}_3\text{CoSb}_2\text{O}_9$, *Nat. Commun.* **9**, 2666 (2018).
- [73] D. Macdougall, S. Williams, D. Prabhakaran, R. I. Bewley, D. J. Voneshen, and R. Coldea, Avoided quasiparticle decay and enhanced excitation continuum in the spin- $\frac{1}{2}$ near-Heisenberg triangular antiferromagnet $\text{Ba}_3\text{CoSb}_2\text{O}_9$, *Phys. Rev. B* **102**, 064421 (2020).
- [74] Q. Zhang and T. Li, Why the Schwinger boson mean field theory fails to describe the spin dynamics of the triangular lattice antiferromagnetic Heisenberg model?, *J. Phys.: Condens. Matter* **33**, 375601 (2021).
- [75] P. Chandra, P. Coleman, and I. Ritchey, Questions, controversies and frustration in quantum antiferromagnetism, *Int. J. Mod. Phys. B* **05**, 171 (1991).
- [76] P. Coleman and P. Chandra, Coleman and Chandra Reply, *Phys. Rev. Lett.* **72**, 1944 (1994).
- [77] A. J. Leggett *et al.*, *Quantum Liquids: Bose Condensation and Cooper Pairing in Condensed-matter Systems* (Oxford University Press, Oxford, 2006).
- [78] The conjugate representations are required to have a singlet ground state of the two-site Heisenberg Hamiltonian.
- [79] J. W. Negele and H. Orland, *Quantum Many-Particle Systems* (CRC Press, Boca Raton, FL, 2018).
- [80] J. Colpa, Diagonalization of the quadratic boson Hamiltonian, *Physica A* **93**, 327 (1978).
- [81] We note that we are choosing condensate states with well-defined parity of the number of SB's. Since the ground states in the even- and odd-parity sectors become degenerate in the thermodynamic limit, it is also possible to choose condensates without a well-defined parity that lead to $\langle b_{j\sigma} \rangle \neq 0$. Given that this choice does not modify the expectation values of physical observables, we work here with condensates with well-defined parity for simplicity.
- [82] O. Penrose and L. Onsager, Bose-Einstein condensation and liquid helium, *Phys. Rev.* **104**, 576 (1956).
- [83] P. Coleman, *Introduction to Many-body Physics* (Cambridge University Press, Cambridge, 2015).
- [84] M. Powalski, G. S. Uhrig, and K. Schmidt, Roton Minimum as a Fingerprint of Magnon-Higgs Scattering in Ordered Quantum Antiferromagnets, *Phys. Rev. Lett.* **115**, 207202 (2015).
- [85] M. Powalski, K. P. Schmidt, and G. Uhrig, Mutually attracting spin waves in the square-lattice quantum antiferromagnet, *SciPost Physics* **4**, 001 (2018).
- [86] O. F. Syljuåsen and H. M. Rønnow, Quantum renormalization of high-energy excitations in the 2D Heisenberg model, *J. Phys.: Condens. Matter* **12**, L405 (2000).
- [87] H. M. Rønnow, D. F. McMorrow, R. Coldea, A. Harrison, I. D. Youngson, T. G. Perring, G. Aeppli, O. Syljuåsen, K. Lefmann, and C. Rischel, Spin Dynamics of the 2d Spin $\frac{1}{2}$ Quantum Antiferromagnet Copper Deuteroformate Tetradeuterate (CFTD), *Phys. Rev. Lett.* **87**, 037202 (2001).
- [88] B. Dalla Piazza, M. Mourigal, N. B. Christensen, G. J. Nilsen, P. Tregenna-Piggott, T. G. Perring, M. Enderle, D. F. McMorrow, D. A. Ivanov, and H. M. Rønnow, Fractional excitations in the square-lattice quantum antiferromagnet, *Nat. Phys.* **11**, 62 (2015).
- [89] D. Yoshioka and J. Miyazaki, Boson mean field theory of the triangular lattice Heisenberg model, *J. Phys. Soc. Jpn.* **60**, 614 (1991).
- [90] C. J. Gazza and H. A. Ceccatto, A Schwinger boson approach to Heisenberg antiferromagnets on a triangular lattice, *J. Phys.: Condens. Matter* **5**, L135 (1993).
- [91] H. A. Ceccatto, C. J. Gazza, and A. E. Trumper, Comment on "Quantum Spin Nematics: Moment-Free Magnetism," *Phys. Rev. Lett.* **72**, 1943 (1994).
- [92] A. O. Scheie, E. A. Ghioldi, J. Xing, J. A. M. Paddison, N. E. Sherman, M. Dupont, D. Abernathy, D. M. Pajerowski, S.-S. Zhang, L. O. Manuel, A. E. Trumper, C. D. Pemmaraju, A. S. Sefat, D. S. Parker, T. P. Devereaux, J. E. Moore, C. D. Batista, and D. A. Tennant, Witnessing quantum criticality

- and entanglement in the triangular antiferromagnet KYbSe₂, [arXiv:2109.11527](#).
- [93] P. A. Maksimov, Z. Zhu, S. R. White, and A. L. Chernyshev, Anisotropic-Exchange Magnets on a Triangular Lattice: Spin Waves, Accidental Degeneracies, and Dual Spin Liquids, *Phys. Rev. X* **9**, 021017 (2019).
- [94] A. Wietek and A. M. Läuchli, Chiral spin liquid and quantum criticality in extended $S = \frac{1}{2}$ Heisenberg models on the triangular lattice, *Phys. Rev. B* **95**, 035141 (2017).
- [95] S.-S. Gong, W. Zhu, J.-X. Zhu, D. N. Sheng, and K. Yang, Global phase diagram and quantum spin liquids in a spin- $\frac{1}{2}$ triangular antiferromagnet, *Phys. Rev. B* **96**, 075116 (2017).